LA-UR- 09-6177

Approved for public release; distribution is unlimited.

Title:	Greenland Ice Sheet surface mass-balance modeling in a 131-year perspective, 1950-2080
Author(s):	Sebastian H. Mernild, LANL; Glen Liston, Colorado State University; Christopher Hiemstra, Colorado State University; and Jens H. Christensen, Danish Meteorological Institute.
Intended for:	Journal of Hydrometeorology

Los Alamos
NATIONAL LABORATORY
EST. 1943

Form 836 (7/06)

Greenland Ice Sheet surface mass-balance modeling in a 131-year perspective, 1950–2080

SEBASTIAN H. MERNILD

Climate, Ocean, and Sea Ice Modeling Group, Computational Physics and Methods, Los Alamos National Laboratory, New Mexico, USA, and International Arctic Research Center and Water & Environmental Research Center, University f Alaska Fairbanks, Alaska, USA

GLEN E. LISTON

Cooperative Institute for Research in the Atmosphere, Colorado State University, Colorado, USA

CHRISTOPHER A. HIEMSTRA

Cooperative Institute for Research in the Atmosphere, Colorado State University, Colorado, USA

JENS H. CHRISTENSEN

Danish Climate Centre, Danish Meteorological Institute, DENMARK

Submitted to Journal of Hydrometeorology 8 December 2008

Re-submitted 12 May 2009

Re-submitted 25 August 2009

Corresponding author address:

Dr. Sebastian H. Mernild

Climate, Ocean, and Sea Ice Modeling Group, Computational Physics and Methods (CCS-2)

Los Alamos National Laboratory,

Los Alamos, New Mexico 87545

USA

E-mail: mernild@lanl.gov

Abstract

Fluctuations in the Greenland Ice Sheet (GrIS) surface mass-balance (SMB) and freshwater influx to the surrounding oceans closely follow climate fluctuations and are of considerable importance to the global eustatic sea level rise. SnowModel, a state-of-the-art snow-evolution modeling system, was used to simulate variations in the GrIS melt extent, surface water balance components, changes in SMB, and freshwater influx to the ocean. The simulations are based on the IPCC scenario A1B modeled by the HIRHAM4 RCM (using boundary conditions from ECHAM5 AOGCM) from 1950 through 2080. *In-situ* meteorological station (GC-Net and WMO DMI) observations from inside and outside the GrIS were used to validate and correct RCM output data before it was used as input for SnowModel. Satellite observations and independent SMB studies were used to validate the SnowModel output and confirm the model's robustness. We simulated a ~90% increase in end-of-summer surface melt extent (0.483×10^6 km^2) from 1950 to 2080, and a melt index (above 2,000-m elevation) increase of 138% (1.96×10^6 km$^2\times$days). The greatest difference in melt extent occured in the southern part of the GrIS, and the greatest changes in the number of melt days was seen in the eastern part of the GrIS (~50–70%) and was lowest in the west (~20–30%). The rate of SMB loss, largely tied to changes in ablation processes, lead to an enhanced average loss of 331 km^3 from 1950 to 2080, an average SMB level of -99 km^3 for the period 2070–2080. GrIS surface freshwater runoff yielded an eustatic rise in sea level from 0.8±0.1 (1950–1959) to 1.9±0.1 mm (2070–2080) sea level equivalent (SLE) y^{-1}. The accumulated GrIS freshwater runoff contribution from surface melting equaled 160 mm SLE from 1950 through 2080.

KEY WORDS Greenland Ice Sheet, HIRHAM4 RCM, runoff, sea level rise, snowmelt extent, SnowModel, surface mass-balance

1. Introduction

The Greenland Ice Sheet (GrIS) is the Northern Hemisphere's largest terrestrial permanent ice- and snow-covered area and a reservoir of water, from a hydrological perspective (e.g., Box et al. 2006, Fettweis 2007, Hanna et al. 2007, Mernild et al. 2008a, 2009a, 2009b), containing between 7.0 to 7.4-m global sea level equivalent (SLE) (Warrick and Oerlemans 1990, Grogory et al. 2004, Lemke et al. 2007). It is essential to predict and assess the impact of future climate on the GrIS, which is believed to be influenced by human activities (IPCC 2001). We must establish the present and future state of the GrIS surface melt extent and surface mass-balance (SMB), including freshwater flux, to detect warning signs indicative of its future response (Hanna et al. 2008). Variability in mass balance closely follows climate fluctuations; the mass balance was close to equilibrium during the relatively cold 1970s and 1980s, and lost mass rapidly as climate warmed in the 1990s and 2000s with no indication of deceleration (Rignot et al. 2008). The GrIS is a useful indicator to ongoing climatic variations and changes, and it is suggested that the GrIS responds more quickly to climate perturbations than previously thought, particularly near the margin in southern Greenland (Velicogna and Wahr 2006).

The climate appears to be changing. Observations indicate that the most pronounced temperature increase occurs at higher northern latitudes, which have increased at almost twice the global average rate in the past 100 years (IPCC 2007). Since 1957, air temperature for the Arctic has increased more than 2°C [http://giss.nasa.gov/]. The warming was accompanied by an increase in precipitation of ~1% decade^{-1} (ACIA 2005). Simulations by Atmosphere-Ocean Models for areas north of 60°N project an increased mean surface air temperature of 2.5°C by the mid-21st century and 4.5 to 5.0°C by the end of the 21st century (ACIA 2005, IPCC 2007).

A response to altered climate has already been observed on the GrIS, manifested by thinning along its periphery (primarily in the south) and a slight thickening of ~2 to 5 cm y^{-1} in the interior (e.g., Krabill et al. 1999, 2000, 2004; Johannessen at al. 2005, Thomas et al. 2006, Zwally et al. 2005). Changes in air temperature result in large changes in the surface melt extent. The GrIS

passive microwave satellite-derived surface melt extent increased 17.6×10^3 km^2 y^{-1} (1973–2007; Mote 2007) and 40.0×10^3 km^2 y^{-1} (1992–2005; Tedesco 2007); and for 2007 a record GrIS melt extent occurred (e.g., Mernild et al. 2009a, 2009b). Further, for the area above 2,000-m elevation the 2007 melt index, defined as the melting area times the number of melting days, was 153% greater than the average for the period 1988–2006, setting a new record (Mote 2007, Tedesco 2007, Mernild et al. 2009b). In contrast to 2007, snowmelt over the whole GrIS in 2008 was not significant at high elevations. Melt extent in 2008 was, however, above the 1979–2007 average, with the 2008 updated melt extent trend of approximately 16×10^3 km^2 y^{-1} (Tedesco et al. 2008).

Numerous GrIS mass-balance studies using airborne laser-altimetry and models (the positive-degree-approach and energy balance) suggest a balance ranging between 25 and -60 km^3 water equivalent (w.eq.) y^{-1} (1961–2003), from -50 to -100 km^3 w.eq. y^{-1} (1993–2003), and reduction at even higher rates between 2003 and 2005, to a loss of ~270 km^3 w.eq. y^{-1} in 2007 (Lemke et al. 2007, Rignot et al. 2008, Mernild et al. 2009b). Analyses of the Gravity Recovery and Climate Experiment (GRACE) satellite data show mass loss of 75 to 129 km^3 w.eq. y^{-1} (2003–2005), and losses ranging from 150 to 270 km^3 w.eq. y^{-1} (2002–2007) (Velicogna and Wahr 2005, 2006, Chen et al. 2006, Lutchke et al. 2006, Ramillien et al. 2006). This indicates an accelerating GrIS mass loss in the 1990s up through the beginning of the 21st century, equivalent to a net global eustatic sea-level rise of ~0.5 mm SLE y^{-1} (Velicogna and Wahr 2006).

Nearly half of the mass lost from the GrIS originates by surface melting and subsequent freshwater runoff into the ocean. The other half is from iceberg calving and geothermal melting (e.g., Lemke et al. 2007, Mernild et al. 2008a). Calculated runoff losses are provided by Janssens and Huybrechts (2000), 281 km^3 y^{-1} (1953–2003); Mote (2003), 278 km^3 y^{-1} (1988–1999); Box et al. (2006), 396 km^3 y^{-1} (1995–2004); Hanna et al. (2008), 351 km^3 y^{-1} (1995–2007); Fettweis (2007), 304 km^3 y^{-1} (1979–2006); Mernild et al. (2008a), 392 km^3 y^{-1} (1995–2005); and Mernild et al. (2009a, 2009b), 397 km^3 y^{-1} (1995–2007). Increases indicate an accelerating GrIS runoff, probably playing a potential role in ocean salinity, sea-ice dynamics, the global eustatic sea level rise (e.g.,

Dowdeswell et al. 1997, ACIA 2005, Box et al. 2006, IPCC 2007), and thermohaline circulation (THC) at the Greenland-Iceland-Norwegian Seas (e.g., Broecker et al. 1985, Broecker and Denton 1990, Su et al. 2006). Accelerating GrIS runoff could perturb the THC by reducing the density contrast driving the circulation (Rahmstorf et al., 2005). Any weakening of the circulation in response to increased GrIS runoff induced by global warming (Gregory et al., 2005, Swingedouw et al., 2006) could reduce heat inflow to the Greenland-Iceland-Norwegian Seas and subsequently reduce the warming in the region, including NW Europe.

This study attempts to improve our quantitative understanding of the past, present, and future (131-year perspective, 1950–2080) GrIS surface melt extent and its related water balance components. Specifically, we address changes in SMB and the influx of freshwater to the ocean as a contribution to the global eustatic sea-level rise. The goal of this study is to apply a well-tested approach – a state-of-the-art modelling system, SnowModel (e.g., Liston and Elder, 2006a, 2006b; Liston et al. 2007; Mernild et al. 2006a, 2008b) to the GrIS for the period 1950 through 2080 based on the IPCC A1B climate scenario. The climate scenario is used in a high resolution Regional Climate Model (RCM) – HIRHAM4 – developed by the Danish Meteorological Institute (DMI) (Christensen et al. 1996, Stendel et al. 2008). The RCM output data was calibrated and tested using *in-situ* meteorological observations obtained from the GrIS (GC-Net; 1995–2005) and the coast (WMO DMI meteorological stations) before being used as meteorological forcings for SnowModel. SnowModel was tested by coincident passive microwave satellite images and SMB studies. We performed the GrIS model simulations for the 131-year period (1950–2080) with the following objectives (1) assess the HIRHAM4 RCM meteorological driving data against *in-situ* meteorological observations; (2) quantify the GrIS end-of-summer maximum surface melt extent and long-term trends; (3) estimate and analyze the GrIS water balance components, including the SMB and freshwater runoff; and (4) quantify the GrIS freshwater runoff and accumulated runoff contribution to global sea level rise.

2. Study area

Greenland is the world's largest island, and the GrIS the Northern Hemisphere's largest terrestrial permanent ice- and snow-covered area (1.834×10^6 km^2), which covers approximately 85% of the island (Figure 1). Greenland is roughly 2,600 km long, up to approximately 950 km wide, and the ice sheet's maximum altitude is more than 3,200 m a.s.l. The total ice sheet volume is 2.85×10^6 km^3, equivalent to an average global sea-level rise between 7.0 to 7.4 m SLE (Warrick and Oerlemans 1990, Grogory et al. 2004, Lemke et al. 2007).

The climate in Greenland is Arctic (Born and Böcher 2001). In the northern parts of the GrIS, winter air temperatures can drop below -70°C, while on the East Greenland land strip, summer temperatures can briefly rise above 25°C (Mernild et al. 2008c). The observed GrIS mean annual air temperature (MAAT) is -13.3°C, covering a non-significant MAAT warming of ~1.8°C for the period 1995–2005 (based on data from the ten coastal meteorological stations; Figure 1 and Table 1, Stations 16 to 25). In southern and southeastern Greenland, the observed annual precipitation is ~2,400 mm w.eq. y^{-1}, while the northern desert-like areas hardly receive any precipitation (<200 mm w.eq. y^{-1}) (e.g., Born and Böcher 2001, Serreze and Barry 2005). Many of the island's characteristics cause considerable contrast in its weather conditions, including complex coastal topography, elevation, distance from the coastal area, marginal glaciers and ice caps, and the GrIS, which makes the climate vary appreciably even over short distances. Temperature inversions are a common feature for Greenland coastal areas (Hansen et al. 2008, Mernild et al. 2008d) and for the GrIS (Putnins 1970).

3. Models and methods

Throughout the Arctic, rough terrain, harsh climatic conditions, and remote locales are commonly cited reasons for lacking knowledge and adequate data. Logistical constraints further make it difficult to collect extensive observations of snow, sublimation, evaporation, and snow and glacier melt. Collecting runoff measurements have typically been considered impossible.

Furthermore, scattered Arctic meteorological stations and limited winter and summer GrIS mass-balance observations, have resulted in sparse and unreliable data related to the spatial and temporal distribution of snow precipitation, sublimation, surface snow and ice melt across much of the GrIS, and runoff to the ocean. Such key components are essential to hydrological research efforts, and there is a clear need to explore issues associated with data sparseness and modeling capabilities.

Likewise, there are several kinds of uncertainties related to climate projections using simulations with coupled atmosphere-ocean GCMs. Apart from uncertainties in future greenhouse gas and aerosol emissions and their conversion to radiative forcings, there are uncertainties in global and, in particular, regional climate responses to these forcings due, for example, to different parameterizations (discussed in detail by Stocker et al. 2001). There is also large natural variability on the regional scale (consider, e.g., the NAO), so that it is difficult to determine which part of the response of a model is due to anthropogenic forcing and to natural variability (solar, volcanic, but also unforced), respectively.

This implies that there is no single ''best'' model to use in an assessment of Arctic (or Greenland) climate changes, although some models clearly perform better than others (e.g., Christensen et al. 2007b, Walsh et al. 2008). However, most of the uncertainties mentioned in the previous paragraph can be quantified by using ensembles of model simulations rather than one particular model. Here, we are limited by the availability of one realisation of a down scaling experiment only, where the behaviour of the driving GCM model is amazingly realistic in describing present day conditions in the Arctic in general and around Greenland in particular (Walsh et al. 2008, Stendel et al. 2008).

3.1 Choosing the model configuration

In order to assess how representative our results may be, given our particular regional-global model set-up, we note as an important starting point, that the ECHAM5 GCM is one of the best performing state-of-the-art models, when it comes to representing the present climate. Walsh et

al. (2008) in their study of GCMs participating in the most recent Coupled Model Intercomparison Project (CMIP) found that for Greenland, the Arctic, and the Northern Hemisphere the ECHAM5 model outperforms most other IPCC class models with respect to all three parameters studied: temperature, precipitation, and mean sea level pressure. In the presence of sea ice, snow coverage and frozen grounds, the interpretation of a climate change signal from GCM simulations is very sensitive to the realism of simulated present day conditions (*e.g.* see Christensen et al. 2007, 2008). Visual inspection of temperature bias maps in Walsh et al. (2008; Figure 8), documents that sea ice coverage for present day conditions in the Arctic is very well depicted by ECHAM5, while most other GCMs tend to show severe biases reflecting either too much or too little sea ice in many locations of the Arctic. In Christensen et al. (2007), the climate change signal for 21 CMIP models (including ECHAM5) are displayed. As pointed out in Christensen et al. (2008), it is interesting to note, however, that the projected climate signals to some degree are caused by quite different mechanisms. Observing in an extract of the performance of model from Walsh et al. (2008), they found a common feature for most of the models, reflected by the ensemble mean, of a clear tendency to simulate too much sea ice in the Barents Sea in winter, with the ECHAM5 model being a clear exception. At the same time, the greatest warming by the end of the century is simulated exactly over this region in the ensemble mean as well as by the individual models. In the NCAR and GFDL models, for example this is partly reflecting the present day bias, while in the ECHAM5 model; this apparently cannot be the case. Furthermore, in general the largest warming occurs in the area with too much ice (strong cold bias) under present day conditions. Thus to some extent, the results at the regional scale are clearly subject to the systematic errors in present day simulations. Using an ensemble of models masks this deficiency. Therefore, maps of warming must be carefully analyzed and cannot be used face value in a region with non-linear feed backs such as in the presence and absence of sea ice.

Given these caveats, we are confident that ECHAM5 based simulations are as good as any possible simulation based on a random choice of GCM. If all GCMs were used for downscaling, the

resulting distribution would partly (perhaps even largely) be due to outlier models with a poor representation of Arctic and Greenlandic climate (especially sea ice) conditions. It is beyond the scope of the present paper to quantify in more details the uncertainty of our results due to the GCM-RCM choice made here.

3.2 HIRHAM4 RCM

The IPCC A2 and B2 climate scenarios (www.ipcc.ch) have been used in the HIRHAM4 RCM (Christensen et al. 1996, 2001; Bjørge et al. 2000; Christensen and Christensen 2007) for several climate change time-slice experiments for present and future conditions, with the HadCM3 AOGCM (atmosphere–ocean general circulation model) (Gordon et al., 2000, Pope et al., 2000) or ECHAM4 AOGCM (Roeckner et al. 1996, Christensen et al. 2007a, 2007b) as boundary conditions. These simulation areas cover central and northern Europe. The performance of the model for Arctic conditions has been found to be state-of-the-art in many aspects (e.g. Christensen and Kuhry 2000, Dethloff et al. 2002, Kiilsholm et al. 2003). In a recent HIRHAM4 study Stendel et al. (2008) has set up the model to conduct a transient climate change experiment representing the period 1950–2080 for the IPCC scenario A1B, covering Greenland and adjacent sea areas (Figure 1). This A1B scenario was run on a 25 km grid-cell increment with 19 vertical levels, using boundary conditions from ECHAM5 AOGCM (Roeckner et al. 2003). While high-resolution regional climate simulations to date mainly have been run as time-slice experiments, we present results of a transient simulation covering 1950–2080. All the forcing data have been taken from the transient ECHAM5-MPI/OM1 run. The A1B experiment, as described in the IPCC AR4 runs (AR4 euqals the Fourth Assessment Report; The runs were done in a world wide coordination with a clearly defined common model setup), begins in 2000 and the AOGCM uses outputs from a detailed simulation of the 20th century experiment as initial conditions in 2000 (e.g., Randall et al. 2007).

Of course, it would be desirable to investigate an ensemble of RCM simulations (different RCMs forced by different GCMs or at realizations of a single GCM, as done in the PRUDENCE

project, see Christensen et al. 2007a). This was, however, impossible due to lack of computer capacity, and so we had to restrict ourselves to this particular configuration. The results from Walsh et al. (2008) indicate that the chosen GCM is a sensible choice, when only one realization can be offered. Deque et al. (2007) indicates that the role of choosing a particular ensemble member is insignificant compared with choosing the GCM.

3.3 SnowModel description

SnowModel (Liston and Elder 2006a) is a spatially distributed snowpack evolution modeling system specifically designed to be applicable over the wide range of snow landscapes, climates, and conditions found around the world. It is made up of four submodels: MicroMet defines the meteorological forcing conditions (Liston and Elder 2006b); EnBal calculates the surface energy exchanges, including melt (Liston 1995, Liston et al. 1999); SnowPack simulates snow depth and water equivalent evolution (Liston and Hall 1995); and SnowTran-3D is a blowing-snow model that accounts for snow redistribution by wind (Liston and Sturm 1998, 2002; Liston et al. 2007). While other distributed snow models exist (e.g. Tarboton et al. 1995, Marks et al. 1999, Winstral and Marks 2002), the SnowTran-3D component allows application in Arctic, alpine (that is, above treeline), and prairie environments that comprise 68% of seasonally snow-covered areas in the Northern Hemisphere (Liston 2004). SnowModel also simulates snow-related physical processes at spatial scales ranging from five meters to global and temporal scales ranging from 10 minutes to a whole season. Simulated processes include: 1) accumulation and loss from snow precipitation, and blowing-snow redistribution; 2) loading, unloading, and blowing-snow sublimation; 3) snow density evolution; and 4) snow pack ripening and melt. SnowModel was originally developed for glacier-free landscapes. For glacier surface mass-balance studies SnowModel was modified to simulate glacier ice melt after winter snow accumulation had ablated (Mernild et al. 2006a, 2007).

3.3.1 MICROMET

MicroMet is a quasi–physically based meteorological distribution model (Liston and Elder 2006b) specifically designed to produce the high-resolution meteorological forcing distributions (air temperature, relative humidity, wind speed, wind direction, precipitation, solar and long-wave radiation, and surface pressure) required to run spatially distributed terrestrial models over a wide range of landscapes in a physically realistic manner. MicroMet uses elevation-related interpolations to modify air temperature, humidity, and precipitation following Kunkel (1989), Walcek (1994), Dodson and Marks (1997), and Liston et al. (1999). Temperature and humidity distributions are defined to be compatible with the observed lapse rates. Wind flow in complex topography is simulated following Ryan (1977) and Liston and Sturm (1998). Solar radiation variations are calculated using elevation, slope, and aspect relationships (Pielke 2002). Incoming long-wave radiation is calculated while taking into account cloud cover and elevation-related variations following Iziomon et al. (2003). Precipitation is distributed following Thornton et al. (1997). In addition, any data from more than one location, at any given time, are spatially interpolated over the domain using a Gaussian distance-dependent weighting function and interpolated to the model grid using the Barnes objective analysis scheme (Barnes 1964, 1973; Koch et al. 1983). Liston and Elder (2006b) and Liston et al. (2007) have performed a rigorous validation of MicroMet using various observational datasets, data denial, and geographic domains. Further, MicroMet has been used to distribute observed and modeled meteorological variables over a wide variety of landscapes in the United States: Colorado (Greene et al. 1999), Wyoming (Hiemstra et al. 2002, 2006), Idaho (Prasad et al. 2001), and Arctic Alaska (Liston et al. 2002, 2007; Liston and Sturm 1998, 2002); Norway: Svalbard and central Norway (Bruland et al. 2004); East Greenland (Mernild et al. 2006a, 2007); the Greenland Ice Sheet (Mernild et al. 2008a, 2008b, 2009a, 2009b); and near-coastal Antarctica (Liston et al. 1999; Liston and Winther 2005). As an example; for the GrIS validations of MicroMet-simulated meteorological data indicate substantial correlation with independent observed GrIS meteorological data from e.g., the Swiss Camp (located within 50 km from JAR1 (Station 7)

at 1,140 m a.s.l. (Table 1; Figure 1)). MicroMet-generated air temperature, relative humidity, and precipitation values account for 84%, 63%, and 69%, respectively, of the variance in the observed 1995–2005 daily averaged dataset. The wind speed has less strong correlations, but the results remain respectable (>50% variance) for representations of GrIS meteorological processes (Mernild et al 2008a).

3.3.2 ENBAL

EnBal performs standard surface energy balance calculations (Liston 1995, Liston et al. 1999). This component simulates surface (skin) temperatures, and energy and moisture fluxes in response to observed and/or modeled near-surface atmospheric conditions provided by MicroMet. Surface latent and sensible heat flux and snowmelt calculations are made using a surface energy balance model of the form:

$$(1 - \alpha)\, Q_{si} + Q_{li} + Q_{le} + Q_h + Q_e + Q_c = Q_m, \qquad (1)$$

where Q_{si} is the solar radiation reaching the earth's surface, Q_{li} is the incoming long-wave radiation, Q_{le} is the emitted long-wave radiation, Q_h is the turbulent exchange of sensible heat, Q_e is the turbulent exchange of latent heat, Q_c is the conductive energy transport, Q_m is the energy flux available for melt, and α is the surface albedo. Details of each term in Equation 1 and the model solution are available in Liston (1995) and Liston et al. (1999). In the presence of snow or glacier ice, surface temperatures greater than 0°C indicate that energy is available for melting. This energy is computed by fixing the surface temperature at 0°C and solving Equation 1 for Q_m. Energy transports towards the surface are defined to be positive.

3.3.3 SNOWPACK

SnowPack is a single-layer, snowpack evolution and runoff/retention model that describes snowpack changes in response to precipitation and melt fluxes defined by MicroMet and EnBal (Liston and Hall 1995, Liston and Elder 2006a). Its formulation closely follows Anderson (1976). In SnowPack, the density changes with time in response to snow temperature and weight of overlying snow (Liston and Elder 2006a). A second density modifying process results from snow melting. The melted snow reduces the snow depth and percolates through the snowpack. If snow temperature is below freezing, any percolating/liquid water refreezes and is stored in the snow (in the 'pores') as internal refreezing. When saturated snow density is reached, assumed to be 550 kg m^{-3} (Liston and Hall 1995), actual runoff occurs. This provides a method to account for heat and mass transfer processes, such as snowpack ripening, during spring melt. The density of new snow from additional accumulation is defined following Anderson (1976) and Liston and Hall (1995). Static-surface (non blowing-snow) sublimation calculated in EnBal is used to adjust the snowpack depth; blowing-snow sublimation is calculated in SnowTran-3D (Liston and Elder 2006a).

3.3.4 SNOWTRAN-3D

SnowTran-3D (Liston and Sturm 1998, Liston et al. 2007) is a three-dimensional submodel that simulates snow depth evolution (deposition and erosion) resulting from windblown snow based on a mass-balance equation that describes the temporal variation of snow depth at each grid cell within the simulation domain. SnowTran-3D's primary components are a wind flow forcing field, a wind shear stress on the surface, snow transport by saltation, snow transport by turbulent suspension, sublimation of saltating and suspended snow, and accumulation and erosion at the snow's surface (Liston and Sturm 2002). Simulated transport and blowing-snow sublimation processes are influenced by the interactions among available snow, topography, and atmospheric conditions (Liston and Sturm 1998). SnowTran-3D simulates snow depth evolution and then uses the snow density simulated by SnowPack to convert it to the more hydrologically significant snow water equivalent (SWE) depth. Deposition and erosion, which lead to changes in snow depth

(Equation 2), are the result of changes in horizontal mass transport rates of saltation, Q_{salt} (kg m^{-1} s^{-1}), changes in horizontal mass transport rates of turbulent suspended snow, Q_{turb} (kg m^{-1} s^{-1}), sublimation of transported snow particles, Q_v (kg m^{-2} s^{-1}), and the water equivalent precipitation rate, P (m s^{-1}). Combined, the time rate of change in snow depth, ζ (m), is

$$\frac{d(\rho_s \zeta)}{dt} = \rho_w P - \left(\frac{dQ_{salt}}{dx} + \frac{dQ_{turb}}{dx} + \frac{dQ_{salt}}{dy} + \frac{dQ_{turb}}{dy}\right) + Q_v \qquad (2)$$

where t (s) is time; x (m) and y (m) are the horizontal coordinates in the west–east and south–north directions, respectively; and ρ_s and ρ_w (kg m^{-3}) are snow and water density, respectively. At each time step, Equation 2 is solved for each individual grid cell within the domain, and is coupled to the neighboring cells through the spatial derivatives (*d/dx, d/dy*). SnowTran-3D simulations have previously been compared against observations in glacier and glacier-free alpine, Arctic, and Antarctic landscapes (Greene et al. 1999, Liston et al. 2000, 2007, Prasad et al. 2001, Hiemstra et al. 2002, 2006, Liston and Sturm 2002, Bruland et al. 2004, Mernild et al. 2006a, 2007, 2008a, 2008b, 2009a, 2009b).

3.3.5 SnowModel input

To solve the equations, SnowModel requires spatially distributed fields of topography and land-cover, and temporally distributed point meteorological data (air temperature, relative humidity, wind speed, wind direction, and precipitation). Meteorological data was obtained from the HIRHAM4 RCM model (1950–2080) based on the IPCC scenario A1B, and from observations from meteorological stations located within the simulation domain (1995–2005). For this study, observed data are obtained from 25 meteorological stations: 15 stations from the Greenland Climate Network (GC-Net), 9 WMO station from the near coast operated by the DMI, and 1 by the Danish National Environmental Research Institute and University of Copenhagen (Figure 1 and Table 1).

Simulations were performed on a one-day time step, although snow- and ice-melt, and blowing snow, are threshold processes that may not be accurately represented by this time step. We recognize that the use of daily-averaged atmospheric forcing variables, instead of hourly values, will produce a smoothing of the natural system. Therefore, daily simulated melt (ablation) and blowing-snow processes (accumulation) were tested against hourly simulated ablation and accumulation values from a test area, the Mittivakkat Glacier (31 km^2), SE Greenland (Mernild and Liston 2009), and remain significant ($p<0.01$; where p is level of significance), with an average difference of 2%, 3%, and 8% for the glacier winter, summer, and net mass-balances, respectively.

Snow precipitation measurements include uncertainties, especially under windy and cold conditions (e.g., Yang et al. 1999, Liston and Sturm 2002, 2004, Serreze and Barry 2005). Solid and liquid precipitation measurements at the DMI meteorological stations (Figure 1 and Table 1; stations 16–18 and 20–25) were calculated from Helman–Nipher shield observations corrected according to Allerup et al. (1998, 2000). Solid (snow) precipitation was calculated from snow-depth sounder observations at the other stations (Figure 1 and Table 1) after the sounder data noise was removed; these data are assumed to be accurate within ±10–15% (Mernild et al. 2007, 2009b). Snow depth sounder observations were partitioned into liquid (rain) precipitation and solid (snow) precipitation at different air temperatures based on methods employed at Svalbard (Førland and Hanssen-Bauer 2003). For air temperatures below -1.5°C, sounder data were considered to represent solid precipitation and for temperatures above 3.5°C precipitation is considered liquid; linear interpolation calculated snow and rain fractions at temperatures between these limits. Snow-depth increases at relative humidity <80% and at wind speed >10 m s^{-1} were removed to better distinguish between the proportions of real snow accumulation based on precipitation events and blowing snow redistribution (Mernild et al. 2007, 2009b). Remaining snow-depth increases were adjusted using a temperature-dependent snow density (Brown et al. 2003) and hourly snowpack settling.

Greenland topographic data for the model simulations were provided by Bamber et al. (2001) who applied "correction" elevations derived by satellite imagery to an existing radar-altimetry digital elevation model (DEM). The image-derived correction was determined from a high-resolution (625 m) grid of slopes inferred from the regional slope-to-brightness relationship of 44 AVHRR images covering all of Greenland (Scambos and Haran 2002). For the model simulations, this time-invariant DEM was aggregated to a 5 km grid-cell increment and clipped to yield a 2,830 by 1,740 km simulation domain that encompassed all of Greenland. The GrIS terminus was confirmed or estimated by using aerial photos and maps (1:250.000 Geodetic Institute, Denmark).

SnowModel is a surface model producing first-order effects of climate change; it does not include glacio-hydro-dynamic and sliding routines. Using a time-invariant DEM could be inappropriate. Therefore, a 1950 through 2080 assessment of GrIS volume, area, and maximum and average heights was performed (Mernild and Greve, unpublished) using SICOPOLIS (SImulation COde for POLythermal Ice Sheets; Greve 1997a, 1997b, 2005), a state-of-the-art 3-d dynamic/thermodynamic shallow-ice approximation model. Based on the IPCC A1B scenario for the period, there was a small change in the GrIS. By 2080 volume differed 3% (5.01×10^4 km^3), melt area changed 8% (4.88×10^4 km^2), and heights shifted <1% (maximum height: 17 m, and average height: 3±(8) m). These discrepancies fall well within the uncertainties of this study. Furthermore, for this study there is only a one-way nesting between HIRHAM4 (the atmosphere) and SnowModel (the surface), not taking e.g., the positive albedo feedback into account associated with snowmelt and the fact that wet snow absorbs as much as 3 times more incident solar energy than dry snow (Steffen 1995).

Each grid cell within the domains was assigned a USGS Land Use/Land Cover System class according to the North American Land Cover Characteristics Database, Version 2.0 (available on-line at [http://edcdaac.usgs.gov/glcc/na_int.html] from the USGS EROS Data Center's Distributed Active Archive Center, Sioux Falls, South Dakota, USA). The snow-holding depth (the snow depth

that must be exceeded before snow can be transported by wind) was assumed to be constant. Albedo was assumed to be 0.8 for snow (Table 2). Realistically, snow albedo changes with time and surface characteristics (Pomeroy and Brun 2001), thus, the model will likely underestimate energy available for surface melting. Therefore, SnowModel simulations with a fixed snow albedo of 0.8 was tested against simulated variable snow albedo from a test area, the Jakobshavn Isbræ drainage area, W Greenland (information about the variable albedo routines see Mernild et al. 2009), indicating a mean annual variable snow albedo of 0.7 (Mernild and Liston, unpublished), and a difference of up to ~15% in SMB and runoff. When the snow is ablated, GrIS surface ice conditions are used. Ice albedo was invariant and assumed to be 0.4. The GrIS ablation zone is characterized by lower albedo on the margin and an increase in albedo toward the ELA, where a veneer of ice and snow dominate the surface (Boggild et al. 2006). The emergence and melting of old ice in the ablation zone creates surface layers of dust (black carbon particles) that were originally deposited with snowfall higher on the ice sheet. This debris cover is often augmented by locally-derived windblown sediment (Boggild et al. 2006). Particles on or melting into the ice change the area-average albedo, increasing melt. User-defined constants for SnowModel are shown in Table 2 (for parameter definitions see Liston and Sturm 1998, 2002). All fjord and ocean areas within the domain were excluded from model simulations. Further, changes in glacier storage based on changes in supraglacial storage (lakes, pond, channels, etc.), englacial storage (ponds and the water table), subglacial storage (cavities and lakes), melt water routing, evolution of a runoff drainage system, and changes based on iceberg calving, tidal response where ice meets ocean, and geothermal melting is not calculated in the SnowModel simulations, even though it might influence the contribution of runoff.

3.4 Satellite images

Detection of surface melt at large spatial scales is effectively accomplished by using satellite microwave data. The daily GrIS snowmelt extent is mapped (25-km grid-cell increment)

using passive microwave satellite observations that discriminate wet from dry snow. The criterion for melt is 1% mean liquid water content by volume in the top meter of snow (Abdalati and Steffen 1997). The center part of the GrIS is the area where the melting threshold of the cross-well ground-penetrating radar microwave algorithm did not show any melt. The end-of-summer maximum observed spatial surface melt distribution at the GrIS was used to validate SnowModel melt simulations.

3.5 HIRHAM4 RCM validation and uncertainty

Before the HIRHAM4 RCM output data can be trusted for use as input data for further modeling, it needs to be tested and calibrated against observed meteorological data as RCM output biases can be large. Stendel and Christensen (2007) provide some basic validation of the current simulation. However, since HIRHAM is running in a full climate mode - i.e. the driving GCM only knows about the state of the atmosphere-ocean system from the external drivers (sun, aerosols and greenhouse gases), whether actually realized (1950–2000) or projected (2001–2080) - we need for our purpose to tie in this single realization with the observed climate system. We have excellent data for verifying SnowModel covering the period 1995–2005. For a bias adjustment or calibration of the HIRHAM results a 10 year period is relatively short, however we have assessed the role of this by an additional calibration in which the model years were 1980–1990 and observed years were 1995–2005. The resulting offset in precipitation is in average 42 mm w.eq. (or 7%) and temperature difference was 1.5°C (or 10%) (1980–1990) with respect to the calibration period (1995–2005). Relative humidity and wind are both insignificantly changed. Mean monthly offset between the RCM modeled output and the observed meteorological data were further estimated for the period 1995–2005 (Figure 2, Table 1; for station information). These mean monthly (1995–2005) offset values were added to the daily RCM meteorological parameters to correct each variable (air temperature, relative humidity, wind speed, and corrected precipitation) for the 1950–2080 period, before being used as meteorological forcings for SnowModel. To assess the performance of the

adjusted SnowModel simulated spatial distributed meteorological data – the spatial distributed meteorological data were tested against *in-situ* meteorological observations (with data not used for calibration) spanning 1995–2005 (see Table 1 for stations used for calibration and validation). We have ranked the data for each period and compared the ranked numbers. This illustrates the ability of HIRHAM to capture the span of realized parameters for the period in concern and therefore also gives a rough estimate about the calibration method. Ideally we should use longer periods and address classical climatological values, but this is beyond the scope of the present work and some of the results are provided elsewhere (e.g., Stendel and Christensen 2007). Validations of the simulated GrIS meteorological data (air temperature, relative humidity, and wind speed) indicate substantial correlation with *in-situ* observed meteorological data from different meteorological stations at the GrIS: JAR1, Humbolt, Saddle, and Summit at different elevations, and with *in-situ* observed precipitation from outside the GrIS: Station Nord, Danmarkshavn, Ittoqqortoormiit, and Ikerasassuaq at different latitudes (Figure 3, Table 1; for station information). Modeled air temperature values account for 98-99% of the variance in the observed 1995–2005 mean monthly dataset. The relative humidity, corrected precipitation, and wind speed have the same or slightly less strong correlations, but results remain respectable for relative humidity (between 85–96%), wind speed (between 83–98%), and for precipitation (between 89–98%), for representations of the GrIS meteorological processes (Figures 3a–d).

The most obvious model bias is the systematic dry bias of the simulated near surface humidity, particularly when humidity is high. This is related to a general difficulty of representing coastal climate on model land points in HIRHAM (Stendel et al. 2008). For precipitation, we note that with the exception of Danmarkshavn, the model captures the span of observed precipitation rather well (perhaps surprisingly so) given the short period of comparison. For temperature, the annual cycle is clearly the dominant feature in the explained variance. However, we also note that the agreement over the full span of temperatures is within what seems to be acceptable for our purpose (see however Stendel et al. 2008)

3.6 SnowModel validation and uncertainty

Few quality observations for spatial *in-situ* snow-evolution, snow and ice surface melt, and glacier net mass-balance are available in Greenland, including from the GrIS. SnowModel accumulation and ablation routines have been tested quantitatively (simulations based on observed meteorological data; for further information see Mernild et al. 2006a, 2006b, 2007, 2008a) at local scale (from East and West Greenland) and regional scale (from the GrIS) using observations from snow pit depths; glacier winter, summer, and net mass-balances; depletion curves; photographic time lapses; satellite images (microwave satellite-derived melt extent); and different parameterizations such as melt index and ELA. A maximum discrepancy between modeled and observed SWE depths of 7%, glacier mass-balances of 7%, snow cover extent of 7%, and GrIS melt discrepancy between melt and non-melt boundaries of 32(±24) km occurs (Mernild et al. 2009a, 2009b). However, in northeastern Greenland the discrepancy can be up to 160 km, where the distances among meteorological stations is far (Figure 1). In this study, SnowModel simulated melt extent were compared against concurrent passive microwave satellite-derived melt extent and previous GrIS SMB studies.

SnowModel, like all models, possesses uncertainties due to processes not represented by the modeling system. For example, routines for simulating the air temperature inversion layer and variable snow and ice albedo are not yet included. In addition, changes in the GrIS area, size, and height according to glacier dynamic processes and subglacial geothermal bottom melting and sliding are not calculated in the model routines. Based on the uncertainties in the modeled results from pervious Greenland SnowModel simulations, including the GrIS, it is reasonable to assume that this GrIS SMB study is influenced with a similar maximum uncertainty of 7% for SWE depth, snow cover extent, and SMB components (Mernild et al. 2006a, 2006b, 2007, 2008a).

4. Results and discussion

Regional Climate Model Trends 1950–2080

Regional Climate Model (RCM) adjusted meteorological data for the 1950–2080 GrIS (air temperature, relatively humidity, wind speed, and precipitation) are illustrated in Figures 4a-d. The GrIS is divided into four sub-areas: I to IV (Figure 4a). The greatest changes in predicted MAAT of 5.6°C occurs in NE Greenland (Area I) (significant; $p<0.01$); this is likely due to the projected change in sea ice extent and thickness particularly off the east coast of Greenland. The lowest warming, 3.6°C, occurs in Area III (significant; $p<0.01$), SW Greenland (Figure 4a), where sea surface temperatures are changing only marginally (see Stendel et al. 2008). Overall, MAAT increased significant 4.8°C from 1950 through 2080 (Figure 4a). Patterns of annual minimum average (1981) and annual maximum average (2080) temperature distribution (Figure 5a) show the variable extent of low interior temperatures (<-20°C) and higher temperatures in coastal Greenland (>0°C). Temporally, the average change in summer (June, July, and August) temperature, temperatures affecting the ablation processes, is 3.1°C (significant; $p<0.01$). Six of the coldest summers occurred in the first decade (1950–1959), while the six warmest summers were in the last decade (2070–2080) of the simulations (Table 3). We note here that this behavior underlines the general aspect of the simulation, namely that the steady warming despite decadal variations is quite robust, which is not likely to be altered if another ECHAM5 ensemble member had been chosen. The average change in summer temperature (3.1°C) is below the average change in MAAT (4.8°C). A winter (December, January, and February) average change of 5.9°C (significant; $p<0.01$) is sizeable. Identical seasonal trends were identified in observations by Box (2002) and Sturm et al. (2005) from 1970s through 1990s.

From 1950–2080 relative humidity increased 1.2% on average (significant; $p<0.01$) (Figures 4b and 5b). Average wind speed decreased slightly <0.1 m s^{-1} (insignificant; $p<0.25$); the largest reduction of -0.2 to -0.5 m s^{-1} occurs at the GrIS northeastern interior (Figures 4c and 5c). Modeled precipitation increased 80 mm w.eq. on the GrIS (significant; $p<0.01$), with the lowest gain of 57 mm w.eq. in NW Greenland (Area IV) and the greatest increase of 160 mm w.eq. in SE

Greenland (significant; $p<0.01$) (Area II; Figures 4d and 5d), due to projected changes in cyclonic systems. The overall trend for predicted climate (1950–2080) is warmer and wetter, where MAAT will increase from -14.8°C (1950–1959) to -10.1°C (2070–2080), and average precipitation from 600 mm w.eq. y^{-1} (1950–1959) to 770 mm w.eq. y^{-1} (2070–2080) (Table 4).

SnowModel Melt Extent Simulations

The simulated end-of-summer GrIS melt extent is illustrated in Figures 6a, 6b, and 6c. To examine annual melt extent spatial variation, 1996 and 2007 were selected randomly from the observation period (1979–2007) and assessment indicates a reasonable degree of similarity between the passive microwave observed and modeled melt distributions (Figure 6a). The differences among spatial annual simulated and observed GrIS melt boundaries average 51(±34) km, with a maximum distance of ~180 km. Modeled end-of-summer maximum melt extent from the observation period are, on average, overestimated by ~10% (Table 4) when compared with satellite observations. The inter-annual discrepancy, likely due to a fixed albedo for snow and ice and a mismatch in modelled and observed resolutions, ranges from ~303,600 km^2 (~17%) in 1998 to ~7,200 km^2 (~1%) in 1991.

The GrIS simulated surface melt and non-melt extent are further shown on decadal basis for the period: 1950–1959 through 2070–2080 (Figure 6b). The average 1950–1959 end-of-summer melt extent was 30% (0.542×10^6 km^2), and 56% for 2070–2080 (1.025×10^6 km^2), indicating an average maximum difference of ~90% (0.483×10^6 km^2). The greatest difference in melt extent occurs in the southern part of the GrIS. To the NW (Area IV) and NE (Area I) of the GrIS the changes in melt extent are less pronounced (Figure 6b). Further, for 1950–1959 and 2070–2080, surface melt occurred at elevations as high as 2,550 and 3,050 m a.s.l., respectively. The distribution of the amount of simulated melt days is further shown for the periods 1950–1959 and 2070–2080 (Figure 6b), indicating a significant average increase of 28 melt days for the GrIS ($R^2=0.74$, $p<0.01$). For the period 1950–1959 the maximum number of melt days was 126, and 242 for 2070–2080. The greatest number of melt days is seen in the south eastern part of the GrIS (Area

II). The largest change in the number of melt days was visible in the eastern part (Area I and II) of the GrIS (~50–70%), and is lower to the west (~20–30%) (Area III and IV) (1950–2080) (Figure 6b). The reason is likely the projected change in sea ice extent and thickness in adjacent seas.

A time series of the simulated end-of-summer GrIS surface melt extent from 1950 through 2080 is illustrated in Figure 6c. The percentage of total modeled melt extent is shown for four years; 1961 (the year with the lowest melt extent in the simulation period: 1950–2080), 1983 (lowest melt extent since the satellite observations began in 1979), 2007 (greatest melt extent since the satellite observations began), and 2077 (the year with the highest melt extent in the simulation period). Simulated melt extent varies from 0.389×10^6 km^2 (21% of the total GrIS area) in 1961 to 1.204×10^6 km^2 (66%) in 2077, indicating an increasing GrIS melt extent through the period.

Water Balance Components

Throughout the year, surface processes such as snow accumulation and redistribution, evaporation, sublimation (including blowing-snow sublimation), and surface melt affect the GrIS water balance (Equation 3). The yearly water balance equation for the GrIS can be described by:

$$P - (E+SU) - R \pm \Delta S = 0 \pm \eta, \qquad (3)$$

where P is the precipitation input from snow and rain (and possible condensation), E is evaporation (liquid to gas phase (atmosphere) flux of water vapor), SU is sublimation (snow blowing; solid to gas phase with no intermediate liquid stage), R is runoff, and ΔS is change in storage (ΔS is also referred as SMB) from changes in glacier storage and snowpack storage. Here η is the water balance discrepancy (error). The error term should be 0 (or small) if the major components (P, ET, SU, R, and ΔS) have been determined accurately. Here, a change in storage is calculated by the residual value.

The RCM-SnowModel SMB precipitation for 1995 through 2004 falls within the range of other studies (Table 5). The greatest average difference is 15 $km^3 y^{-1}$ and is not surprising given vast uncertainties in measuring snow precipitation. Measuring snow precipitation typically includes errors, especially under windy and cold conditions (e.g., Yang et al. 1999, Liston and Sturm 2002, 2004, Serreze and Barry 2005). Snow-fall in the Arctic is most often connected with strong winds and typically takes the form of fine snowflakes (Sturm et al. 1995). As a result, wind easily lifts and redistributes the snowflakes according to exposure and local topography, and it is sometimes difficult to distinguish between a period of snow-fall and a period of drifting snow.

RCM-SnowModel simulated GrIS runoff estimate (1995–2004; Table 5) was highest compared to the other studies. The maximum difference was 59 $km^3 y^{-1}$and the minimum difference was 3 $km^3 y^{-1}$. SnowModel runoff routines take retention and internal refreezing into account when meltwater penetrates through the snowpack. These routines do have a significant effect on the SMB runoff. The role of meltwater retention in terms of the overall GrIS mass-balance indicates that runoff is overestimated between 20–29% if no retention/refreezing routines are included (1995–2004) (Mernild et al. 2008b). The overestimation corresponds with previous values of ~25% estimated by Janssens and Huybrechts' (2000) single-layer snowpack model (used by e.g. Hanna *et al.*, 2002, 2005, 2008; Table 5). The lack of retention/refreezing routines in SnowModel (used in this paper and Mernild et al. 2008; Table 5) leads to an overestimation of ocean runoff, a consequent overestimation of global sea level rise, and may explain the larger difference among SnowModel simulated runoff and the other studies.

For SMB (1995–2004), the average RCM-SnowModel simulated values were lowest, 32 $km^3 y^{-1}$ lower than Mernild et al. (2008a; a study based on observed data only) and 51 $km^3 y^{-1}$ lower than Box et al. (2006). Compared with the study by Hanna et al. (2008), the RCM-SnowModel SMB was 207 $km^3 y^{-1}$ lower. The lower SnowModel simulated GrIS SMB values are due to the incorporation of evaporation and sublimation values of 142 $km^3 y^{-1}$ in the SMB calculations (see Equation 1), where sublimation alone accounts for 64 $km^3 y^{-1}$ in average: a value in the lower end

of Box and Steffen's (2001) observed GrIS sublimation values of 62(±23) to 120(±65) $km^3\ y^{-1}$ (1995–2000). SnowModel simulated evaporation and sublimation accounted for 26% for the total GrIS ablation processes, indicating variations in the range from 134 $km^3\ y^{-1}$ in 2003 to 153 $km^3\ y^{-1}$ in 1999.

Table 4 presents the decadal GrIS surface melt conditions and the water balance components (Equation 3), for the period 1950 through 2080. The melt index (the area above 2,000-m elevation where the greatest changes in melting occur) increased 138% (1.96×10^6 $km^2\times$days), and the end-of-summer maximum melt extent grew 89% (4.83×10^5 km^2). The trend in melt extent is illustrated in Figure 6c. Over time, more of the GrIS surface area melted going from 0.542×10^6 km^2 (1950–1959) to 1.025×10^6 km^2 (2070–2080) and the melting occurred for a longer duration during the ablation season. Increasing decadal temperatures largely explain the variance between MAAT and melt extent (R^2=0.79) and melt index (R^2 = 0.89), indicating that rising temperatures influence the ablation processes and melt conditions.

Modeled ELA provides a useful metric of accumulation and ablation's net influence on the SMB (Table 4). On the GrIS from 1950–2080, the decadal ELA is changing in elevation from 1,150 to 2,060 m a.s.l.; an average elevation increase of ~70 m a.s.l. $decade^{-1}$. Values of ELA correlate highly with MAAT (R^2=0.94, $p<0.01$) and with precipitation (R^2=0.73, $p<0.01$) (Table 4). Location of the ELA is largely tied to changes in MAAT and subsequent changes in melt extent and melt index. The spatial location of ELA is influenced by local topography, regional variations in precipitation regimes, dominant cyclonic systems, and latitude.

The SMB trend from 1950–2080 (Figure 7; Table 4) integrates accumulation (snow precipitation) and ablation (evaporation, sublimation, and runoff) over the GrIS. It is the manifestation of increased precipitation and ablation.

Interannual variability in precipitation and ablation caused sizeable SMB fluctuations with correlations of R^2=0.46, $p<0.01$, and R^2=0.93, $p<0.01$, respectively (Table 4). SMB fluctuations were largely tied to changes in ablation processes. Fluctuation patterns illustrated on Figure 7,

which were almost identical to the trends described by Rignot et al. (2008), indicated the highest balance in the 1970s and early 1980s with subsequent rapid losses as temperatures warmed. In Table 4 the inter-decadal trend and variability in precipitation (R^2=0.73, $p<0.01$), evaporation/sublimation (R^2=0.85, $p<0.01$), runoff (R^2=0.94, $p<0.01$), and SMB (R^2=0.86, $p<0.01$) rates possessed significantly high correlations throughout the simulation period. Precipitation rose 133 km^3, evaporation/sublimation 73 km^3, and runoff 391 km^3, leading to enhanced average SMB losses of 331 km^3 (Figure 7). Throughout the simulation period the decadal SMB varied from 256 (1960–1969) to -99 $km^3\ y^{-1}$ (2070–2080), averaging 79(±129) $km^3\ y^{-1}$ (Table 4). SMB values below zero (negative SMB-value) occur from the period 2040–2049 through 2070–2080 (Table 4). A negative SMB developed in response to high ablation values (Table 4), ranging from an average 706 $km^3\ y^{-1}$ (of which 74% was runoff) for 2040–2049, to 870 $km^3\ y^{-1}$ (of which 77% was runoff) in 2070–2080. Our SMB is similar to Fettweis et al.'s (2008) SMB loss estimates generated from mean SMB values of twenty-four AOGCMs (using projections of temperature and precipitation anomalies from AOGCMs) performed for the IPCC Fourth Assessment Report for 2010–2080. The RCM SnowModel simulated SMB is, on average, ~180 $km^3\ y^{-1}$ below the AOGCMs mean values and is similar to the lowest AOGCMs 2080 projected SMB of -100 $km^3\ y^{-1}$.

Sublimation plays an important role in the annual high latitude hydrological cycle. Previous GrIS studies (e.g., Box and Steffen 2001, Mernild et al 2008a) have both shown that as much as 12–23% of the annual precipitation may be returned to the atmosphere by sublimation. In Arctic North America, studies by Liston and Sturm (1998, 2004), Essery et al. (1999), and Pomeroy and Essery (1999) indicate that 5–50% of the annual solid precipitation was returned to the atmosphere by sublimation. For the GrIS (1950–2080), modeled annual sublimation averaged 74 $km^3\ y^{-1}$, which is ~47% of the total average for evaporation and sublimation of 158 $km^3\ y^{-1}$ (Table 4), and is 12% of the total precipitation of 677 $km^3\ y^{-1}$. SnowModel simulated results were in the lower end of Box and Steffen's (2001) observed GrIS sublimation values of 62(±23) to 120(±65)

$km^3\ y^{-1}$ (12 to 23% of the total precipitation), even through the observed values are from the period 1995 through 2000.

The average GrIS runoff from the period 1950 through 2080 is 442(±134) $km^3\ y^{-1}$ (Table 4 and Figure 7). During this time runoff accelerated ~30 km^3 $decade^{-1}$ to a runoff value of 668 $km^3\ y^{-1}$ (2070–2080). The average GrIS runoff of 442 $km^3\ y^{-1}$ is comparable to approximately 1,000 icebergs (density: 917 kg m^3) with dimensions 1 km × 1 km with an ice thickness of 500 m. The GrIS runoff equals a specific runoff of 7.6(±2.3) $l\ s^{-1}\ km^{-2}\ y^{-1}$, which is equivalent to an average rise in global eustatic sea level of 1.2 mm SLE y^{-1}, changing from 0.8±0.1 (1950–1959) to 1.9±0.1 mm SLE y^{-1} (2070–2080) (Table 4 and Figure 7). The accumulated GrIS freshwater runoff is 160 mm SLE from 1950 through 2080. In addition to enhanced runoff, GrIS may shed mass by iceberg calving and geothermal melting. Thus, simulated GrIS freshwater runoff might underestimate the mass lost by half (Lemke et al. 2007, Mernild et al. 2008b).

In terms of our general satisfaction with these model results, it is important to be clear about the assumptions and potential deficiencies of this modeling study. In these simulations we have assumed a mean monthly offset value corrected to each meteorological variable, a time-invariant DEM, a fixed albedo for snow and ice, and no routines for the influence of air temperature inversions on snowmelt and glacier mass-balance simulations. We also recognize that the use of daily-averaged atmospheric forcing variables will produce a smoothing of the natural system compared with higher temporal resolutions. Our understanding of the GrIS freshwater flux to the ocean is still far from complete. Detailed climate-cryospheric interactions are being examined at finer scales at the GrIS Kangerluassuaq drainage area, West Greenland, to estimate the freshwater influx to the ocean before upscaling routines to the entire GrIS.

5. Summary and conclusion

These GrIS simulations reveal continued warming and dramatically increased ablation amount and extent from 1950–2080. Over the period of simulation, surface runoff increased from

285 km^3 y^{-1} (1950–1959) to 668 km^3 y^{-1} (2070–2080). The GrIS freshwater runoff will be a factor in global sea-level rise, equivalent to an average rise of 1.2 mm SLE y^{-1}, and a cumulative increase of around 160 mm SLE in this particular model setup under an IPCC A1B emission scenario.

Realistic simulations are required to better predict GrIS SMB loss and the impacts of this loss for the North Atlantic Ocean, since it plays an important role in determining the global thermohaline circulation, salinity, sea-ice dynamics, and the global eustatic sea level rise. There is a high degree of agreement between GrIS simulations and recorded observations, as well as simulated GrIS SMB values and previous modeling studies. However, SnowModel doesn't yet include routines for variable snow albedo and routines for the influence of air temperature inversions on snowmelt and glacier mass-balance simulations. These improvements are forthcoming and will likely bolster modeling efforts. In this work we have not considered feedback processes from a changing GrIS to the atmosphere, which are likely also to influence simulated surface air temperatures and thereby impact the resulting melt rates.

Another uncertainty which we have partly ignored here is the spread in model projections of the climate of the future. We acknowledge that more than twenty IPCC type GCMs have been analyzed with respect to their projection in climate change, *i.e.* by the IPCC (Christensen et al., 2007) showing a wide range of results with the Arctic exhibiting an even higher lack of confidence than any other region. We attribute a substantial part of this uncertainty to imperfections of various models, particularly with respect to the representation of Arctic processes. In our work we employed only one model, which we have identified as one of (if not) the best GCMs in representing present climate conditions, ECHAM5. This model simulates a future climate not far diverged from the ensemble mean of 21 IPCC class models. Our results presented here are representative of state-of-the-art modeling, but not comprehensive in assessing the entire range of possibilities.

Acknowledgement

Very special thanks to the three anonymous reviewers for their insightful critique of this article. This work was supported by grants from the University of Alaska Presidential IPY Postdoctoral Foundation and the University of Alaska Fairbanks (UAF) Office of the Vice Chancellor for Research and conducted during the first author's IPY Post Doc. Program at the UAF. Special thanks to the Faculty of Science and Institute of Low Temperature Science, Hokkido University, Japan, for hosting the first author from April through July, and to Colorado State University, Cooperative Institute for Research in the Atmosphere, for hosting the first author through September and October 2008, and February 2009. Thanks to Martin Stendel and John Cappelen at the Danish Meteorological Institute (DMI) for providing HIRHAM4 RCM data and WMO meteorological data obtained from the near coast, and to the Cooperative Institute for Research in Environmental Science (CIRES), University of Colorado at Boulder, for providing meteorological data from the Greenland Climate Network (GC-Net) automatic weather stations. Also thanks to Theodore Scambos, CIRES, University of Colorado at Boulder, for providing the Greenland digital elevation model.

References

Abdalati, W. and K. Steffen 1997. The apparent effects of the Mt. Pinatubo eruption on the Greenland ice sheet melt extent. *Geophys. Res. Lett.*, 24: 1795–1797.

Abdalati W. and K. Steffen 2001. Greenland ice sheet melt extent: 1979–1999, *J. Geophys. Res.*, 106: 33983–3389.

ACIA, 2005. Arctic Climate Impact Assessment. Cambridge University Press, 1042 p.

Allerup, P., H. Madsen, and F. Vejen, 1998. Estimating true precipitation in arctic areas. Proc. Nordic Hydrological Conf., Helsinki, Finland, Nordic Hydrological Programme Rep. 44: 1–9.

Allerup, P., H. Madsen, and F. Vejen, 2000. Correction of precipitation based on off-site weather information. *Atmos. Res.*, 53: 231–250.

Anderson, E. A., 1976. A point energy balance model of a snow cover. NOAA Tech. Rep. NWS 19, 150 pp.

Bamber, J., S. Ekholm, and W. Krabill, 2001. A new, highresolution digital elevation model of Greenland fully validated with airborne laser altimeter data. *J. Geophys. Res.*, 106B: 6733–6746.

Barnes, S. L., 1964. A technique for maximizing details in numerical weather map analysis. *J. Appl. Meteor.*, 3: 396–409.

Barnes, S. L., 1973. Mesoscale objective analysis using weighted timeseries observations. NOAA Tech. Memo. ERL NSSL-62, National Severe Storms Laboratory, Norman, OK, 60 pp.

Boggild, C. E., S. G. Warren, R. E. Brandt, and K. J. Brown 2006. Effects of dust and black carbon on albedo of the Greenland ablation zone. Abstract: American Geophysical Union, Fall Meeting 2006, abstract #U22A-05.

Box, J. E., 2002. Survey of Greenland instrumental temperature records: 1973–2001. *Int. Climatol.*, 22: 1829–1847.

Box, J. E., D. H. Bromwich, B. A. Vennhuis, L.-S. Bai, J. C. Stroeve, J. C. Rogers, K. Steffen, T. Haren, and S.-H. Wang, 2006. Greenland ice sheet surface mass balance variability (1988-2004) from calibrated Polar MM5 output. *Journal of Climate*, 19: 2783–2800.

Box, J. E. and K. Steffen, 2001: Sublimation estimates for the Greenland ice sheet using automated weather station observations. *J. Geophys. Res.,* 106 (D24): 33965–33982.

Born, E. W. and J. Böcher, 2001. The ecology of Greenland. Nuuk. Ministry of Environment and Natural Resources. 429 pp.

Bjørge D., J. E. Haugen, T. E. Nordeng 2000. Future climate in Norway. *DNMI Research Report* No. 103, Norwegian Meteorological Institute, Oslo, Norway (ISSN 0332–9879).

Broecker, W. S., and G. H. Denton, 1990. The role of ocean-atmosphere reorganization in glacial cycles. *Quaternary Science Reviews*, 9: 305–341.

Brown, R. D., B. Brasnett, and D. Robinson, 2003. Gridded North American monthly snow depth and snow water equivalent for GCM evaluation. *Atmos.–Ocean*, 41: 1–14.

Broecker, W. S., D. M. Peteet, and D. Rind, 1985. Does the ocean-atmosphere system have more than one stable mode of operation. *Nature,* 315: 21–26.

Bruland, O., G. E. Liston, J. Vonk, K. Sand, and A. Killingtveit, 2004. Modelling the snow distribution at two High-Arctic sites at Svalbard, Norway, and at a Sub-Arctic site in Central Norway. Nordic Hydrology, 35(3): 191–208.

Chen, J. L., C. R. Wilson, and D. B. Tapley, 2006. Satellite gravity measurements confirm accelerated melting of Greenland ice sheet, Science, 313: 1958–1960.

Christensen, J. H., T. R. Carter, M. Rummukainen, and G. Amanatidis, 2007a. Evaluating the performance and utility of regional climate models: the PRUDENCE project, Climatic Change, 81 Supl. 1, 1-6,DOI:10.1007/s10584-006-9211-6.

Christensen, J. H. and O. B. Christensen, 2007. A summary of the PRUDENCE model projections of changes in European climate by the end of this century, *Climatic Change*, 81 Supl. 1, 7-30, DOI:10.1007/s10584-006-9210-7.

Christensen, J. H., O. B. Christensen, P. Lopez, E. van Meijgaard, and M. Botzet, 1996: The HIRHAM4 Regional Atmospheric Climate Model; DMI Scientific Report 96-4. [Available from DMI, Lyngbyvej 100, Copenhagen Ø, DENMARK].

Christensen J. H., O. B. Christensen, J-P. Schultz, S. Hagemann, and M. Botzet, 2001. High resolution physiographic data set for HIRHAM4: an application to a 50 km horizontal resolution domain covering Europe. *DMI Technical Report*, 01–15.

Christensen, J. H., B. Hewitson, A. Busuioc, A. Chen, X. Gao, I. Held, R. Jones, R. K. Kolli, W.-T. Kwon, R. Laprise, V. Magaña Rueda, L. Mearns, C. G. Menéndez, J. Räisänen, A. Rinke, A. Sarr and P. Whetton, 2007b: Regional Climate Projections. In: Climate Change 2007. The Physical Science Basis. Contribution of Working Group I to the Fourth Assessment Report of the Intergovernmental Panel on Climate Change [Solomon, S., D. Qin, M. Manning, Z. Chen, M. Marquis, K. B. Averyt, M. Tignor and H. L. Miller (eds.)]. Cambridge University Press, Cambridge, United Kingdom and New York, NY, USA.

Christensen J. H. and P. Kuhry, 2000: High resolution regional climate model validation and permafrost simulation for the East-European Russian Arctic. *J. Geophys. Res.*, 105: 29647–29658.

Christensen, J. H., M., Stendel, P., Kuhry, P., V. Romanovsky, J., Walsh, 2008. Does permafrost deserve attention in comprehensive climate models? NICOP, Fairbanks, Alaska. Pp. 247–250.

Déqué, M., D. P. Rowell, D. Lüthi, F. Giorgi, J. H. Christensen, B. Rockel, D. Jacob, E. Kjellström, M. de Castro, and B. van den Hurk, 2007: An intercomparison of regional climate simulations for Europe: assessing uncertainties in model projections, *Climatic Change,* 81 Supl. 1: 53–70, doi:10.1007/s10584-006-9228-x

Dethloff, K., M. Schwager, J. H. Christensen, S. Kiilsholm, A. Rinke, W. Dorn, F. Jung-Rothenhäusler, H. Fischer, S. Kipfstuhl, H. Miller, 2002: Recent Greenland accumulation estimated from regional climate model simulations and ice core analysis, *J. Clim.*, 15: 2821–2832.

Dodson, R., and D. Marks, 1997. Daily air temperature interpolation at high spatial resolution over a large mountainous region. *Climate Res.*, 8: 1–20.

Dowdeswell, J. A., J. O. Hagen, H. Björnsson, A. F. Glazovsky, W. D. Harrison, P. Holmlund, J. Jania, R. M. Koerner, B. Lefauconnier, C. S. L. Ommanney, and R. H. Thomas, 1997. The Mass balance of Circum-Arctic Glaciers and Recent Climate Change. *Quaternary Research* 48, 1–4, no. QR971900: 1–14.

Essery, R. L. H., L. Li, and J. W. Pomeroy, 1999: A distributed model of blowing snow over complex terrain. *Hydrol. Processes,* 13: 2423–2438.

Fettweis, X. 2007. Reconstruction of the 1979–2006 Greenland ice sheet surface mass balance using the regional climate model MAR. *The Cryosphere*, 1: 21–40.

Fettweis, X., E. Hanna, H. Gallée, P. Huybrechts, and M. Erpicum, 2008. Estimation of the Greenland ice sheet surface mass balance for the 20th and 21st centuries, The *Cryosphere*, 2: 117–129.

Førland, E. J. and I. Hanssen-Bauer, 2003. Climate variations and implications for precipitations types in the Norwegian Arctic. Met. Report, Norwegian Meteorological Institute, Report No. 24/02, 21 pp.

Gordon C., C. Cooper, C. A. Senior, H. Banks, J. M. Gregory, T. C. Johns, J. F. B. Mitchell, R. A. Wood, 2000. The simulation of SST, sea ice extents and ocean heat transports in a version of the Hadley Centre coupled model without flux adjustments. *Climate Dynamics* 16: 147–168.

Greene, E. M., G. E. Liston, and R. A. Pielke, 1999. Simulation of above treeline snowdrift formation using a numerical snowtransport model. *Cold Reg. Sci. Technol.*, 30: 135–144.

Greve, R. 1997a. Application of a polythermal three-dimensional ice sheet model to the Greenland ice sheet: response to a steady-state and transient climate scenarios, *Journal of Climate*, 10(5): 901–918.

Greve, R. 1997b. A continuum-mechanical formulation for shallow polythermal ice sheets, Phil. *Trans. R. Soc. Lond. A*, 355: 921–974.

Greve, R. 2005. Relation of measured basal temperatures and the spatial distribution of the geothermal flux for the Greenland ice sheet, *Annals of Glaciology*, 42: 424–432.

Gregory, J., K. Dixon, R. J. Stouffer, A. Weaver, E. Driesschaert, M. Eby, T. Fichefet, H. Hasumi, A. Hu, J. Jungclaus, I. Kamenkovich, A. Levermann, M. Montoya, S. Murakami, S. Nawrath, A. Oka, A. Solokov, and R. Thorpe, 2005. A model intercomparison of changes in the Atlantic thermohaline circulation in response to increasing atmospheric concentration, *Geophys. Res. Lett.*, 32, L12703, doi:10.1029/2005GL023209.

Gregory, J. M., P. Huybrechts, and S. C. B. Raper, 2004. Threatened loss of the Greenland ice-sheet. *Nature*, 428: 616.

Hanna, E., P. Huybrechts, and T. Mote, 2002. Surface mass balance of the Greenland ice sheet from climate-analysis data and accumulation/runoff models. *Annals of Glaciology*, 35: 67–72.

Hanna, E., P. Huybrechts, I. Janssens, J. Cappelen, K. Steffen, and A. Stephens, 2005. Runoff and mass balance of the Greenland ice sheet: 1958–2003. *J. Geophys. Res.*, 110: 1–16.

Hanna, E., J. Box, and P. Huybrechts 2007. Greenland Ice Sheet mass balance. Arctic Report Card 2007, update to State of Arctic Report 2006, NOAA, available online at http://www.arctic.noaa.gov/reportcard/

Hanna, E., P. Huybrechts, K. Steffen, J. Cappelen, R. Huff., C. Shuman, T. Irvine-Fynn, S. Wise, and M. Griffiths, 2008. Increased Runoff from melt from the Greenland Ice Sheet: A response to Global Warming. *Journal of Climate*, 21: 331–341.

Hanna, E., J. Cappelen, X. Fettweis, P. Huybrechts, A. Luckman, M. H. Ribergaard 2009. Hydrologic response of the Greenland Ice sheet: the role of oceanographic warming. *Hydrological Processes*, 23: 7–30.

Hansen, B. U., C. Sigsgaard, L. Rasmussen, J. Cappelen, J. Hinkler, S. H. Mernild, D. Petersen, M. Tamstorf, M. Rasch, and B. Hasholt, 2008. Present Day Climate at Zackenberg. *Advances in Ecological Research*, 40: 115–153.

Hiemstra, C. A., G. E. Liston, and W. A. Reiners, 2002. Snow Redistribution by Wind and Interactions with Vegetation at Upper Treeline in the Medicine Bow Mountains, Wyoming. *Arctic, Antarctic, and Alpine Research*, 34: 262–273.

Hiemstra, C. A., G. E. Liston, and W. A. Reiners, 2006. Observing, modelling, and validating snow redistribution by wind in a Wyoming upper treeline landscape. *Ecological Modelling*, 197: 35–51.

Hasholt, B., G. E. Liston, and N. T. Knudsen, 2003. Snow distribution modelling in the Ammassalik region, southeast Greenland. *Nordic Hydrol.*, 34: 1–16.

IPCC, 2001. Summary for policy makers: a report of working Group I of the International Panel on Climate Change. Geneva, World meteorological Organisation; United Nations Environment Programme. Intergovernmental Panel on Climate Change.

IPCC, 2007. Summary for Poicymakers. In: Climate Change 2007: The Physical Science Basis. Contribution of Working Group I to the Fourth Assessment Report of the Intergovernmental Panel on Climate Change [Solomon, S., D. Qin, M. Manning, Z. Chen, M. Marquis, K. B. Averyt, M. Tignor and H.L. Miller (eds.)]. Cambridge University Press, Cambridge, United Kingdom and New York, USA.

Iziomon, M. G., H. Mayer, and A. Matzarakis, 2003. Downward atmospheric longwave irradiance under clear and cloudy skies: Measurement and parameterization. *J. Atmos. Sol.-Terr. Phys.*, 65: 1107–1116.

Janssens, I., and P. Huybrechts, 2000. The treatment of meltwater retention in Mass-balance parameterisation of the Greenland Ice Sheet, *Annals of Glaciology*, 31: 133–140.

Johannessen, O. M., K. Khvorostovsky, M. W. Miles, and L. P. Bobylev, 2005. Recent ice sheet growth in the interior of Greenland, *Sciencexpress*: 1013–1016, doi:10.1126/science.1115356.

Kiilsholm, S., J. H. Christensen, K. Dethloff, and A. Rinke, 2003: Net accumulation of the Greenland Ice Sheet: Modelling Arctic regional climate change. *Geoph. Re. Lett.*, 30, 10.1029/2002GL015742

Koch, S. E., M. DesJardins, and P. J. Kocin, 1983. An interactive Barnes objective map analysis scheme for use with satellite and conventional data. *J. Climate Appl. Meteor.*, 22: 1487–1503.

Krabill, W., W. Abdalati, E. Frederick, S. Manizade, C. Martin, J. Sonntag, R. Swift, R. Thomas, W. Wright, J. Yungel. 2000. Greenland Ice Sheet: High-Elevation Balance and Peripheral Thinning. *Science,* 289. 5478: 428–430. DOI: 10.1126/science.289.5478.428.

Krabill, W., E. Frederick, S. Manizade, C. Martin, J. Sonntag, R. Swift, R. Thomas, W. Wright, J. Yungel. 1999. Rapid Thinning of Parts of the Southern Greenland Ice Sheet. *Science*, 283, 5407: 1522–1524. DOI: 10.1126/science.283.5407.1522

Krabill, W., and Coauthors, 2004. Greenland Ice Sheet: Increased coastal thinning. *Geophys. Res. Lett.,* 31, L24402, doi:10.1029/2004GL021533.

Kunkel, K. E., 1989: Simple procedures for extrapolation of humidity variables in the mountains western United States. *J. Climate*, 2: 656–669.

Lemke, P., J. Ren, R.B. Alley, I. Allison, J. Carrasco, G. Flato, Y. Fujii, G. Kaser, P. Mote, R.H. Thomas and T. Zhang, 2007. Observations: Changes in Snow, Ice and Frozen Ground. In: *Climate Change 2007: The Physical Science Basis. Contribution of Working Group I to the Fourth Assessment Report of the Intergovernmental Panel on Climate Change* [Solomon, S., D. Qin, M. Manning, Z. Chen, M. Marquis, K.B. Averyt, M. Tignor and H.L. Miller (eds.)]. Cambridge University Press, Cambridge, United Kingdom and New York, NY, USA.

Liston, G. E., 1995. Local Advection of Momentum, Heat, and Moisture during the Melt of Patchy Snow Covers. *Journal of Applied Meteorology*, 34(7): 1705–1715.

Liston, G. E., 2004. Representing subgrid snow cover heterogeneities in regional and global models. *J. Climate*, 17: 1381–1397.

Liston, G. E., and K. Elder, 2006a. A distributed snow-evolution modeling system (SnowModel). *Journal of Hydrometeorology*, 7: 1259–1276.

Liston, G. E., and K. Elder, 2006b. A meteorological distribution system for high resolution terrestrial modeling (MicroMet). *Jounal of Hydrometeorology*, 7: 217–234.

Liston, G. E., and D. K. Hall 1995. An energy-balance model of lake-ice evolution. *J. Glaciol.*, 41: 373–382.

Liston, G. E., R. B. Haehnel, M. Sturm, C. A. Hiemstra, S. Berezovskaya, and R. D. Tabler, 2007. Simulating complex snow distributions in windy environments using SnowTran-3D. *Journal of Glaciology*, 53: 241–256.

Liston, G. E., and D. K. Hall, 1995. An energy-balance model of lake-ice evolution. *J. Glaciol.*, 41: 373–382.

Liston, G. E., J. P. McFadden, M. Sturm, and R. A. Pielke Sr., 2002. Modeled changes in arctic tundra snow, energy, and moisture fluxes due to increased shrubs. *Global Change Biol.*, 8: 17–32.

Liston, G. E., and M. Sturm, 1998. A snow-transport model for complex terrain. *J. Glaciol.* 44: 498–516.

Liston, G. E., and M. Sturm, 2002. Winter Precipitation Patterns in Arctic Alaska Determined from a Blowing-Snow Model and Snow-Depth Observations. *Journal of Hydrometeorology*, vol. 3: 646–659.

Liston, G. E., and M. Sturm, 2004: The role of winter sublimation in the Arctic moisture budget. *Nord. Hydrol.*, 35: 325–334.

Liston, G. E., and J.-G. Winther, 2005. Antarctic Surface and Subsurface Snow and Ice Melt Fluxes. *Journal of Climate*,18: 1469–1481.

Liston, G. E., J.-G. Winther, O. Bruland, H. Elvehøy, and K. Sand, 1999. Below surface ice melt on the coastal Antarctic ice sheet. *J. Glaciol.*, 45(150): 273–285.

Lutchke, S. B., et al. 2006. Recent Greenland ice mass loss by drainage system from satellite gravity observations, *Science*, 314: 1286–1289.

Marks, D., J. Domingo, D. Susong, T. Link, and D. Garen, 1999. A spatially distributed energy balance snowmelt model for application in mountain basins. *Hydrol. Processes*, 13: 1935–1959.

Mernild, S. H., B. Hasholt, B. H. Jakobsen, and B. U. Hansen, 2008d. Climatic conditions at the Mittivakkat Glacier catchment (1994–2006), Ammassalik Island, SE Greenland, and in a 109 years term perspective (1898–2006). *Danish Journal of Geography,* 108(1): 51–72.

Mernild, S. H., B. Hasholt, and G. E. Liston, 2006b. Water flow through Mittivakkat Glacier, Ammassalik Island, SE Greenland. *Danish Journal of Geography*, 106(1): 25–43.

Mernild, S. H., Hasholt, B., and Liston, G. 2008c Climatic control on river discharge simulations, Zackenberg River Drainage basin, NE Greenland. *Hydrological Processes*, 22: 1932–1948. DOI: 10.1002/hyp.6777.

Mernild, S. H. and G. E. Liston, 2009. The influence of air temperature inversions on snowmelt and glacier mass-balance simulations, Ammassalik Island, SE Greenland. In review *Journal of Applied Meteorology and Climatology.*

Mernild, S. H., G. E. Liston, and B. Hasholt, 2007. Snow-Distribution and Melt Modeling for Glaciers in Zackenberg River Drainage Basin, NE Greenland. *Hydrological Processes*. 21: 3249–3263. DOI: 10.1002/hyp.6500.

Mernild, S. H., G. E. Liston, and B. Hasholt, 2008b. East Greenland freshwater runoff to the Greenland-Iceland-Norwegian Seas 1999–2004 and 2071–2100. *Hydrological Processes*. DOI: 10.1002/hyp.7061.

Mernild, S. H., Liston, G. E., Hasholt, B. and Knudsen, N. T. 2006a. Snow distribution and melt modeling for Mittivakkat Glacier, Ammassalik Island, SE Greenland. *Journal of Hydrometeorology*, 7: 808–824.

Mernild, S. H., G. E. Liston, C. A., Hiemstra, and K. Steffen, 2008a. Surface Melt Area and Water Balance Modeling on the Greenland Ice Sheet 1995–2005. *Journal of Hydrometeorology*. doi: 10.1175/2008JHM957.1.

Mernild, S. H., G. E. Liston, C. A. Hiemstra, and K. Steffen, 2009a. Record 2007 Greenland Ice Sheet surface melt-extent and runoff. *Eos Trans. AGU*, 90(2): 13–14.

Mernild, S. H., G. E. Liston, C. A. Hiemstra, K. Steffen, E. Hanna, and J. H. Christensen, 2009b. Greenland Ice Sheet surface mass-balance modeling and freshwater flux for 2007, and in a 1995–2007 perspective. *Hydrological Processes*, DOI: 10.1002/hyp.7354.

Mernild, S. H., G. E. Liston, D. L. Kane, N. T. Knudsen, and B. Hasholt, 2008e. Snow, runoff, and mass-balance modeling for entire Mittivakkat Glacier (1998–2006), Ammassalik Island, SE Greenland. *Danish Journal of Geography*, 108(1): 121–136.

Mote, T. L., 2003. Estimations of runoff rates, mass balance, and elevation changes on Greenland ice sheet from passive microwave observations. *J. Geophys. Res.,* 108(D2), 4052.

Mote, T. L. 2007. Greenland surface melt trends 1973–2007: Evidence of a large increase in 2007. *Geophysical Research Letters*, vol. 34, L22507, doi:10.1029/2007GL031976.

Pielke, R. A., Sr., 2002. Mesoscale Meteorological Modeling. Academic Press, 676 pp.

Pomeroy, J.W. and E. Brun. 2001. "Physical properties of snow" In, (eds. H.G. Jones, J.W. Pomeroy, D.A. Walker and R.W. Hoham) Snow Ecology: an Interdisciplinary Examination of Snow-covered Ecosystems. Cambridge University Press, Cambridge, UK. 45–118 .

Pomeroy, J. W., and R. L. H. Essery, 1999: Turbulent fluxes during blowing snow: Field test of model sublimation predictions. *Hydrol. Processes,* 13: 2963–2975.

Pope V. D., M. L. Gallani, P. R. Rowntree, R. A. Stratton, 2000. The impact of new physical parametrizations in the Hadley Centre climate model—HadAM3. *Climate Dynamics* 16: 123–146.

Prasad, R., D. G. Tarboton, G. E. Liston, C. H. Luce, and M. S. Seyfried, 2001. Testing a blowing snow model against distributed snow measurements at Upper Sheep Creek. *Water Resour. Res.*, 37: 1341–1357.

Putnins, P. 1970. The climate of Greenland, in Climates of the Polar Regions, World Surv. of Climatol., vol. 12, edited by S. Orvig, pp. 3–112, Elsevier Sci., New York.

Ramillien, G., A. Lombard, A. Cazanave, E. R. Ivins, M. Llubes, F. Remy, and R. Biancala, 2006. Interannual variations of the mass balance of the Antarctic and Greenland ice sheet from GRACE. *Glob. Planet. Change,* 53: 198–208.

Rahmstorf, S., M. Crucifix, A. Ganopolski, H. Goosse, I. Kamenkovich, R. Knutti, G. Lohmann, R. Marsh, L. A. Mysak, Z. Wang, and A. J. Weaver, 2005. Thermohaline circulation hysteresis: A model intercomparison, *Geophys. Res. Lett.*, 32(23), L23605, doi:10.1029/2005GL023655.

Randall, D.A., Wood, R.A., Bony, S., Colman, R., Fichefet, T., Fyfe, J., Kattsov, V., Pitman, A., Shukla, J., Srinivasan, J., StouVer, R. J., Sumi, A., et al. (2007) In: Climate Change 2007: The Physical Science Basis (Ed. by S. Solomon, D. Qin, M. Manning, Z. Chen, M. Marquis, K.B. Averyt, M. Tignor and H. L. Miller). Cambridge University Press, Cambridge.

Rignot, E., J. E. Box, E. Burgess, and E. Hanna. 2008. Mass balance of the Greenland ice sheet from 1958 to 2007. *Geophysical Research Letters*, 35, L20502, doi:10.1029/2008GL035417.

Roeckner, E., K. Arpe, L. Bengtsson, M. Christoph, M. Claussen, L. Dümenil, M. Esch, M. Giorgetta, U. Schlese and U. Schulzweida, 1996. The atmospheric general circulation model

ECHAM-4: Model description and simulation of present-day climate. Rep. 218, Max-Planck-Inst. Für Meteorologie, Hamburg, Germany.

Roeckner E., G. Bäuml, L. Bonaventura, R. Brokopf, M. Esch, M. Giorgetta, S. Hagemann, I. Kirchner, L. Kornblueh, E. Manzini, A. Rhodin, U. Schlese, U. Schulzweida and A. Tompkins, 2003. The atmospheric general circulation model ECHAM 5. Part I: Model description, *MPI Rep* vol. 349, Max Planck Institute for Meteorology, Hamburg.

Ryan, B. C., 1977. A mathematical model for diagnosis and prediction of surface winds in mountains terrain. *J. Appl. Meteor.*, 16: 1547–1564.

Scambos, T. and T. Haran 2002. An image-enhanced DEM of the Greenland Ice Sheet. *Annals of Glaciology*, 34: 291–298.

Serreze, M. C. and Barry R.G., 2005. The Arctic Climate System. Cambridge Atmospheric and Space Science Series: Cambridge; p. 424.

Steffen, K. 1995. Surface energy exchange during the onset of melt at the equilibrium line altitude of the Greenland ice sheet. *Ann. Glaciology,* 21: 13–18.

Stendel, M., J. H. Christensen, and D. Petersen, 2008. Arctic Climate and Climate Change with a Focus on Greenland, *Adv. in Eco. Res.*, 40, 13–43, DOI: 10.1016/S0065-2504(07)00002-5.

Stocker, T. F., Clarke, G. K. C., Le Treut, H., Lindzen, R.S., Meleshko, V. P., Mugara, R. K., Palmer, T. N., Pierrehumbert, R. T., Sellers, P. J., Trenberth, K. E. and Willebrand, J., 2001. In: Climate Change 2001: The Scientific Basis (Ed. By J.T. Houghton, Y. Ding, D.J. Griggs, M.

Noguer, P.J. van der Linden, X. Dai, K. Maskell and C.A. Johnson), pp. 418–470. Cambridge University Press, Cambridge.

Sturm, M., J. Holmgren, and G. E. Liston, 1995. Seasonal Snow Cover Classification System for Local to Global Applications. *J. Climate* 8: 1261–1283.

Sturm, M., J. Schimel, G. Michaelson, J. M. Welker, S. F. Oberbauer, G. E. Liston, J. Fahnestock, and V. E. Romanovsky, 2005. Winter biological processes could help convert Arctic tundra to shrubland. *Bioscience,* 55: 17–26.

Su, F., J. C. Adam, K. E. Trenberth, and D. P. Lettenmaier, 2006. Evaluation of surface water fluxes of the pan-Arctic land region with a land surface model and ERA-40 reanalysis. *Journal of Geophysical Research*, Vol. 111, D05110, doi: 10.1029/2005JD006387.

Swingedouw, D., P. Braconnot, and O. Marti, 2006. Sensitivity of the Atlantic Meridional Overturning Circulation to the melting from northern glaciers in climate change experiments, *Geophys. Res. Lett.*, 33, L07711, doi:10.1029/2006GL025765.

Tedesco, M. 2007. Greenland Ice Sheet snowmelt from spaceborne microwave brightness temperatures. *Eos Trans. AGU*, 88: 238.

Tedesco, M., X. Fettweis, M. Broeke, R. Wal, and P. Smeets 2008. Extremt Snowmelt in Northern Greenland During Summer 2008. *Eos Trans. AGU*, 89: 391.

Tarboton, D. G., T. G. Chowdhury, and T. H. Jackson, 1995. A spatially distributed energy balance snowmelt model. Biogeochemistry of Seasonally Snow-Covered Catchments, K. A. Tonnessen, M. W. Williams, and M. Tranter, Eds., *IAHS Publication,* 228: 141–155.

Thomas, R., E. Frederick, W. Krabill, S. Manizade, and C. Martin, 2006. Progressive increase in ice loss from Greenland, *Geophys. Res. Lett.*, 33, L10503, doi:10.1029/2006GL026075.

Thornton, P. E., S. W. Running, and M. A. White, 1997: Generating surfaces of daily meteorological variables over large regions of complex terrain. *J. Hydrol.*, 190: 214–251.

Velicogna, I. and J. Wahr, 2005. Greenland mass balance from GRACE, *Geophys. Res. Lett.*, 32, L18505, doi:10.1029/2005GL023955.

Velicogna, I., and J. Wahr 2006. Acceleration of Greenland ice mass loss in spring 2004, *Nature*, 443: 329–331.

Warrick, R., and J. Oerlemans, 1990. Sea level rise. *Climate Change: The IPCC Scientific Assessment,* J. T. Houghton, G. J. Jenkins, and J. J. Ephraums, Eds., Cambridge University Press, 261–281.

Walcek, C. J., 1994. Cloud cover and its relationship to relative humidity during a spring midlatitude cyclone. *Mon. Wea. Rev.*, 122: 1021–1035.

Walsh, J. E., W. L. Chapman, V. Romanovsky, J. H. Christensen and M. Stendel, 2008. Global Climate Model Performance over Alaska and Greenland, *J. Clim.*, 21: 2156–2174, doi:10.1175/2008JCLI2163.1

Winstral, A., and D. Marks, 2002: Simulating wind fields and snow redistribution using terrain-based parameters to model snow accumulation and melt over a semi-arid mountain catchment. *Hydrol. Processes*, 16: 3585–3603.

Yang, D., Ishida, S., Goodison, B.E. and Gunther, T. 1999. Bias correction of precipitation data for Greenland. *Journal of Geophysical Research-Atmospheres*, 104, (D6): 6171–6181.

Zwally, J. H., Giovinetto, M., Li, J., Cornejo, H., Beckley, M., Brenner, A., Saba, J., and Yi, D. 2005. Mass changes of the Greenland and Antarctic ice sheets and shelves and contributions to sea-level rise: 1992–2002, *J. Glaciol.*, 51(175): 509–527.

Figure 1: The HIRHAM4 RCM Greenland simulation domain, including the GrIS, and the location of the meteorological stations (used for calibration and validation): the GC-Net meteorological stations from the GrIS and the WMO meteorological stations from near the coast. The Figure is based on a study by Stendel et al. (2008).

Figure 2: Observed and HIRHAM4 RCM simulated meteorological data (25 km grid cell): (a) air temperature; (b) relative humidity; (c) wind speed; and (d) precipitation for the period 1995 through 2005 (see Figure 1 and Table 1 for stations used for calibration). The mean monthly offset between the observed and the modeled values is illustrated and used for calibration of HIRHAM RCM modeled values for the period 1950 through 2080.

Figure 3: A comparison between ranked monthly observed meteorological data and ranked HIRHAM4-MircoMet/SnowModel-simulated data for the period 1995 through 2005: a) mean air temperature; b) mean relative humidity; c) mean wind speed; and d) precipitation. For air temperature, relative humidity, and wind speed four meteorological stations at different elevations on the GrIS were used: Humbolt (no 3), Summit (no 4), JAR1 (no 7), and Saddle (no 8), and for precipitation four meteorological stations at different latitude were used: Station Nord (no 17), Danmarkshavn (no 18), Ittoqqorotoormiit (no 20), and Ikerasassuaq (no 22). Only monthly precipitation values above 0 mm w.eq. were included. For additional station information and data time period see Table 1.

Figure 4: HIRHAM4 RCM calibrated anomaly time series and average changes for the GrIS sub-area 1 to 4 from 1950 through 2080 for: (a) air temperature; (b) relative humidity; (c) wind speed; and (d) precipitation. For all four parameters the zero-line is included, and R^2 and p (level of significance). The inset figure in (a) indicates the division of the GrIS into sub-area I to IV.

Figure 5: Greenland HIRHAM4 RCM calibrated annual minimum average, annual maximum average, and average annual trend difference from 1950 through 2080 for the parameters: (a) air

temperature, (b) relative humidity, (c) wind speed, and (d) precipitation. The years for the annual minimum and maximum are mentioned for each parameter.

Figure 6a: The GrIS maximum melt extent based on passive microwave satellite-derived observations and SnowModel simulations for the years 1996 (second lowest melt extent since the satellite observations began in 1979 (only 1992 is smaller than the 1996-melt extent) and 2007 (greatest melt extent since the satellite observations began). The simulated melt extent includes number of days with surface melt.

Figure 6b: Average maximum decadal melt extent from 1950–1959 through 2070–2080, including the number of days with surface melt.

Figure 6c: Time series for the simulated GrIS surface melt extent from 1950 through 2080. The percentage of total modeled melt extent is shown for the four years: 1961 (the year with the lowest melt extent in the simulation period: 1950–2080), 1983 (lowest melt extent since the satellite observations began in 1979), 2007 (greatest melt extent since the satellite observations began), and 2077 (the year with the highest melt extent in the simulation period).

Figure 7: Time series for the simulated GrIS precipitation (P), evaporation and sublimation (E+SU), surface mass-balance (ΔS), runoff (R), and annual and accumulated contribution to the global sea level change for the period 1950–2080.

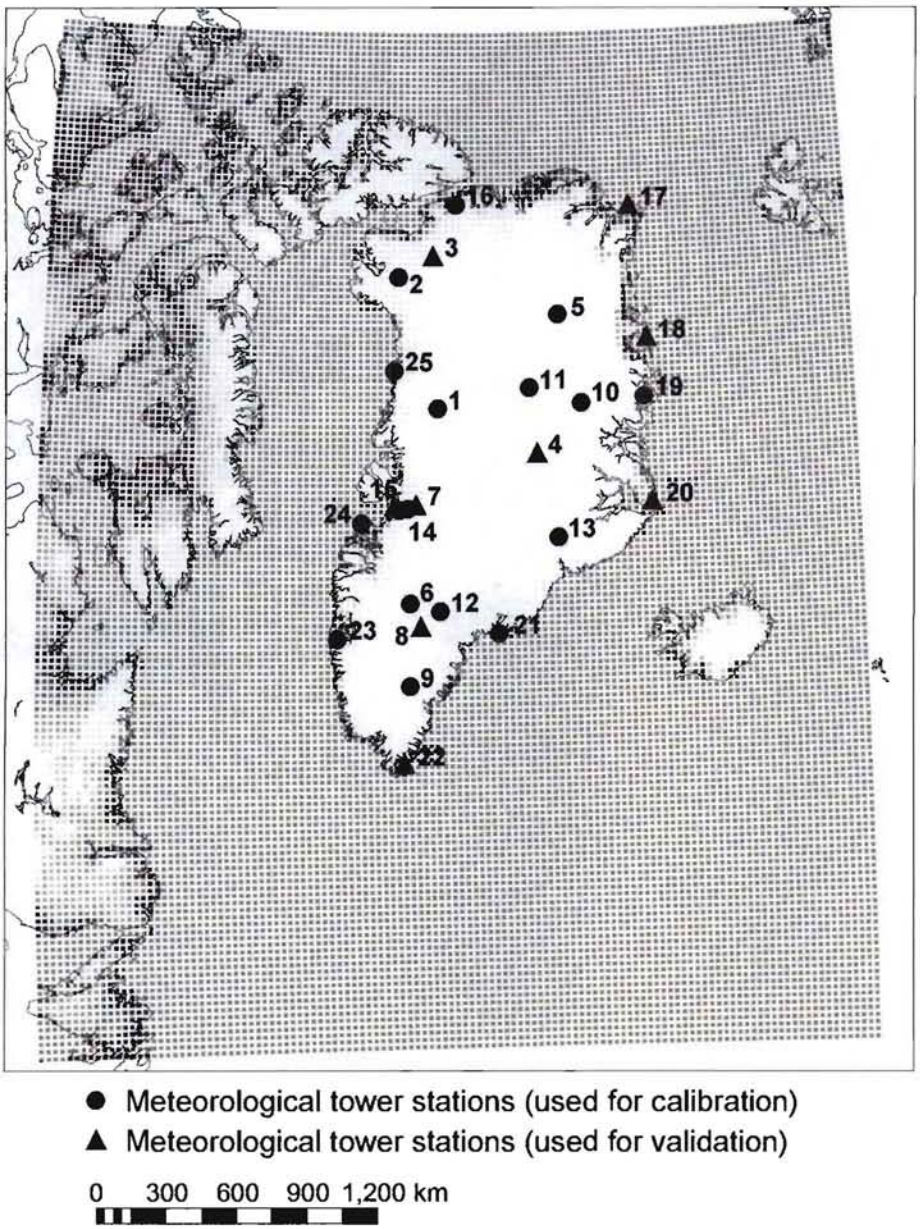

Figure 1: *The HIRHAM4 RCM Greenland simulation domain, including the GrIS, and the location of the meteorological stations (used for calibration and validation): the GC-Net meteorological stations from the GrIS and the WMO meteorological stations from near the coast. The Figure is based on a study by Stendel et al. (2008).*

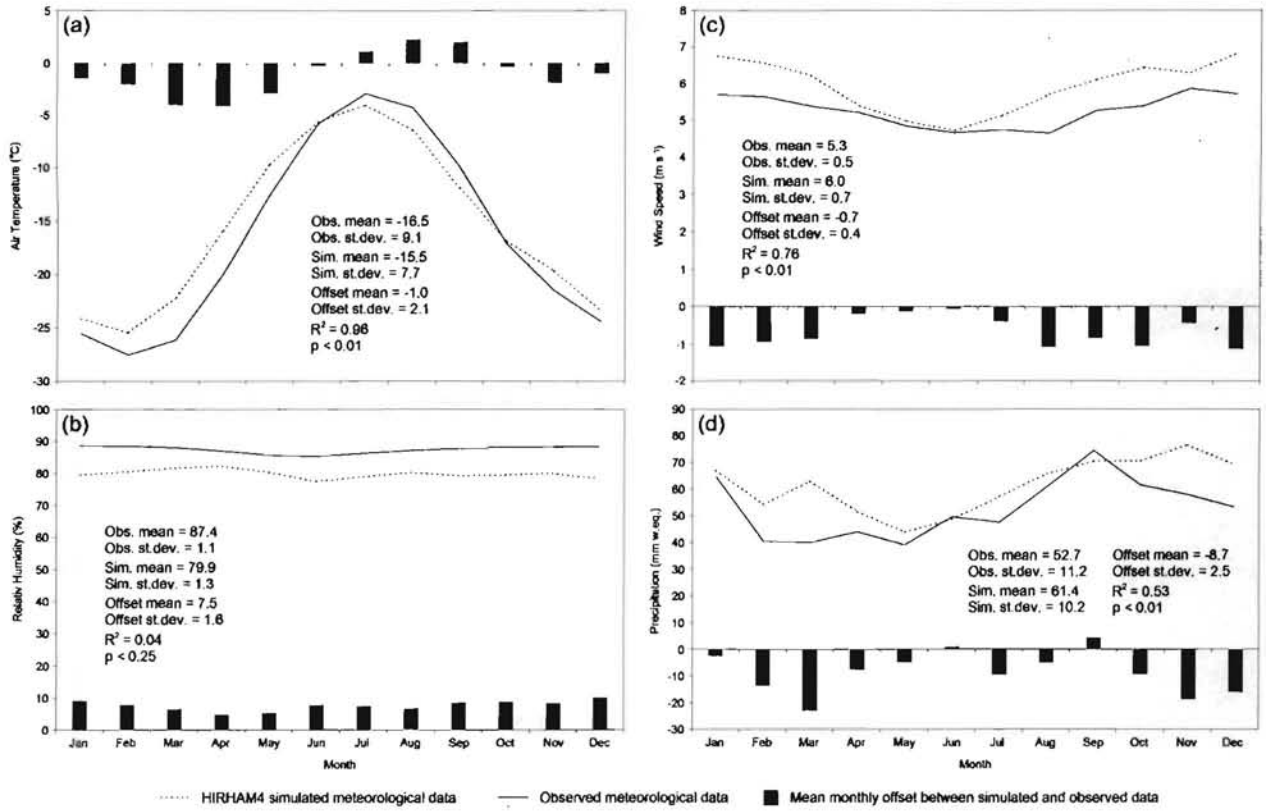

Figure 2: *Observed and HIRHAM4 RCM simulated meteorological data (25 km grid cell): (a) air temperature; (b) relative humidity; (c) wind speed; and (d) precipitation for the period 1995 through 2005 (see Figure 1 and Table 1 for stations used for calibration). The mean monthly offset between the observed and the modeled values is illustrated and used for calibration of HIRHAM RCM modeled values for the period 1950 through 2080.*

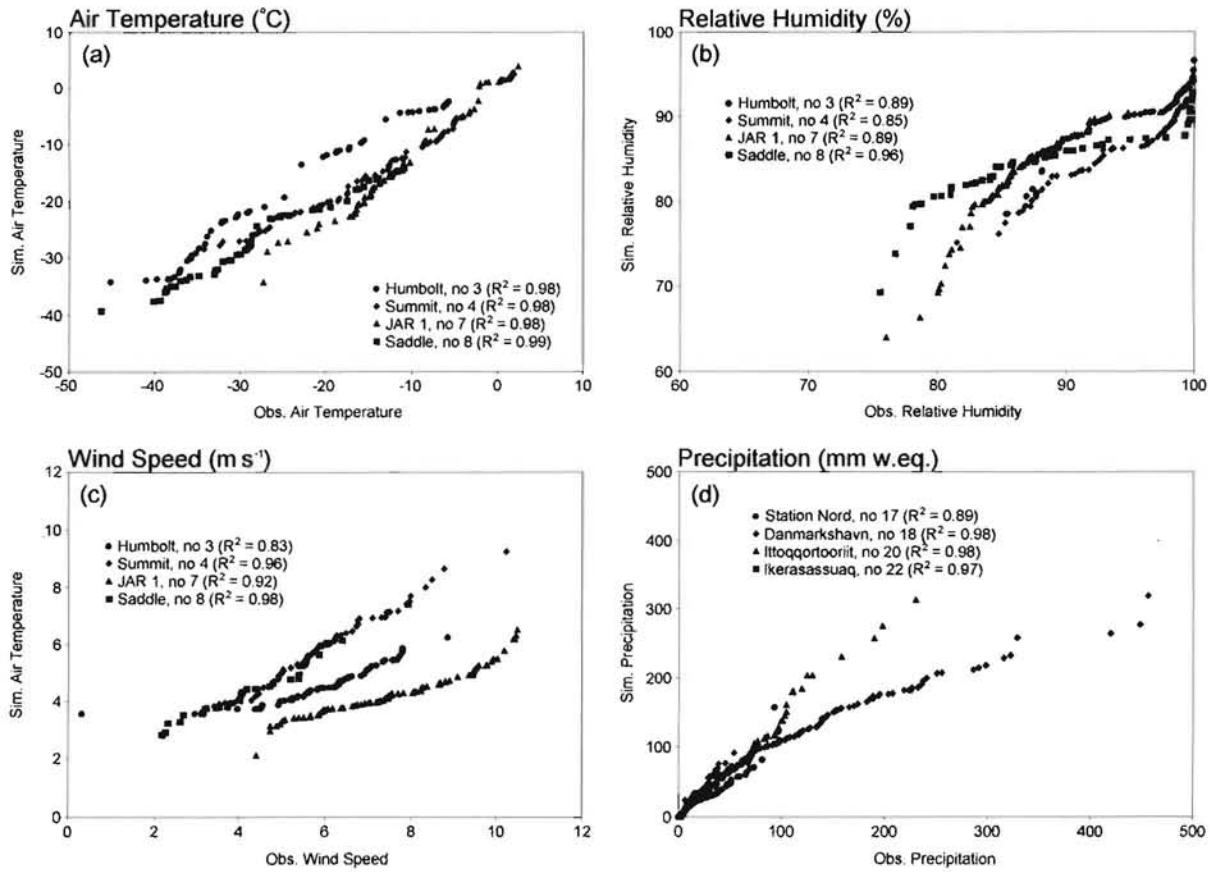

Figure 3: *A comparison between ranked monthly observed meteorological data and ranked HIRHAM4-MircoMet/SnowModel-simulated data for the period 1995 through 2005: a) mean air temperature; b) mean relative humidity; c) mean wind speed; and d) precipitation. For air temperature, relative humidity, and wind speed four meteorological stations at different elevations on the GrIS were used: Humbolt (no 3), Summit (no 4), JAR1 (no 7), and Saddle (no 8), and for precipitation four meteorological stations at different latitude were used: Station Nord (no 17), Danmarkshavn (no 18), Ittoqqorotoormiit (no 20), and Ikerasassuaq (no 22). Only monthly precipitation values above 0 mm w.eq. were included. For additional station information and data time period see Table 1.*

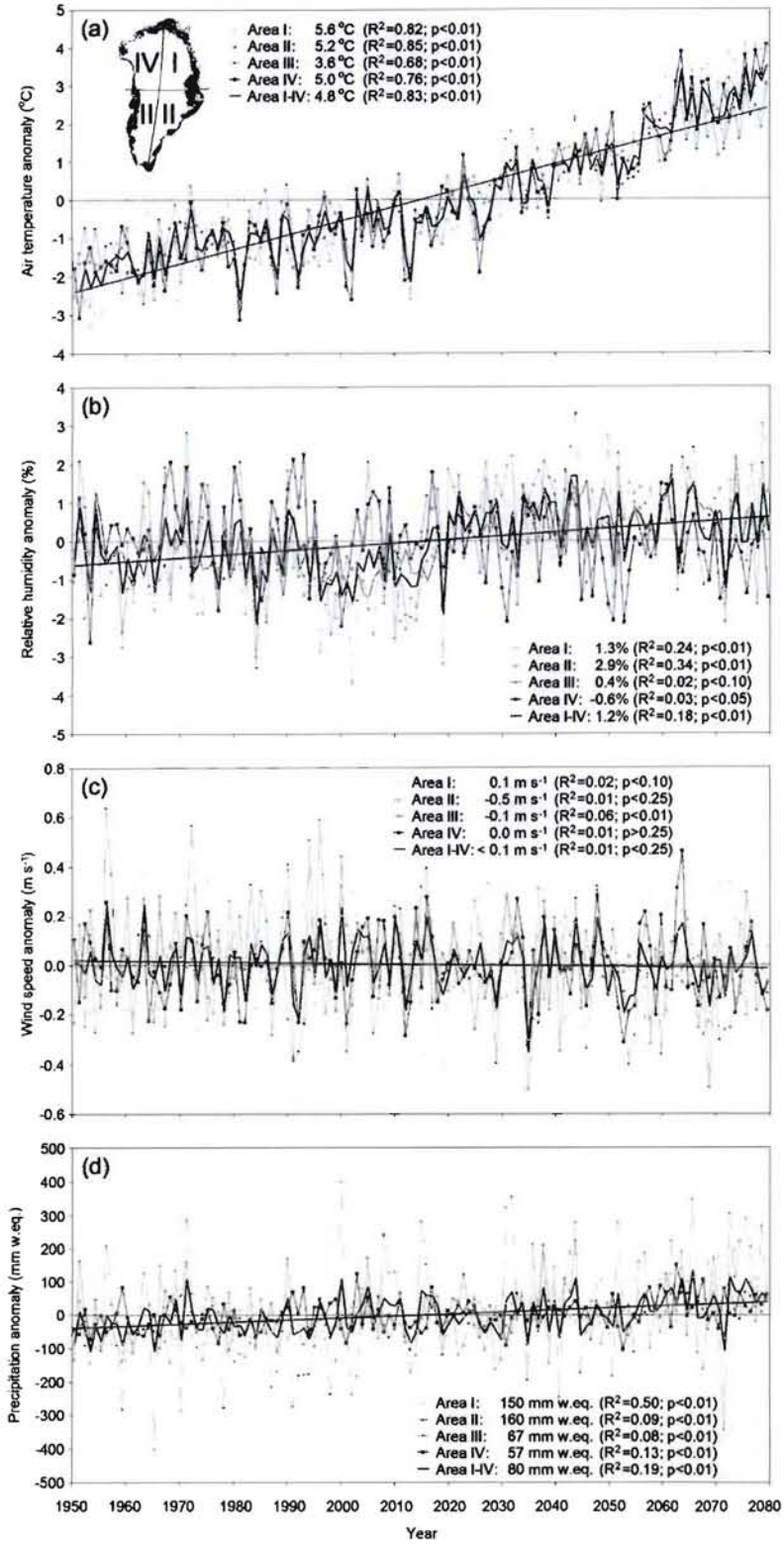

Figure 4: *HIRHAM4 RCM calibrated anomaly time series and average changes for the GrIS sub-area 1 to 4 from 1950 through 2080 for: (a) air temperature; (b) relative humidity; (c) wind speed; and (d) precipitation. For all four parameters the zero-line is included, and R^2 and p (level of significance). The inset figure in (a) indicates the division of the GrIS into sub-area I to IV.*

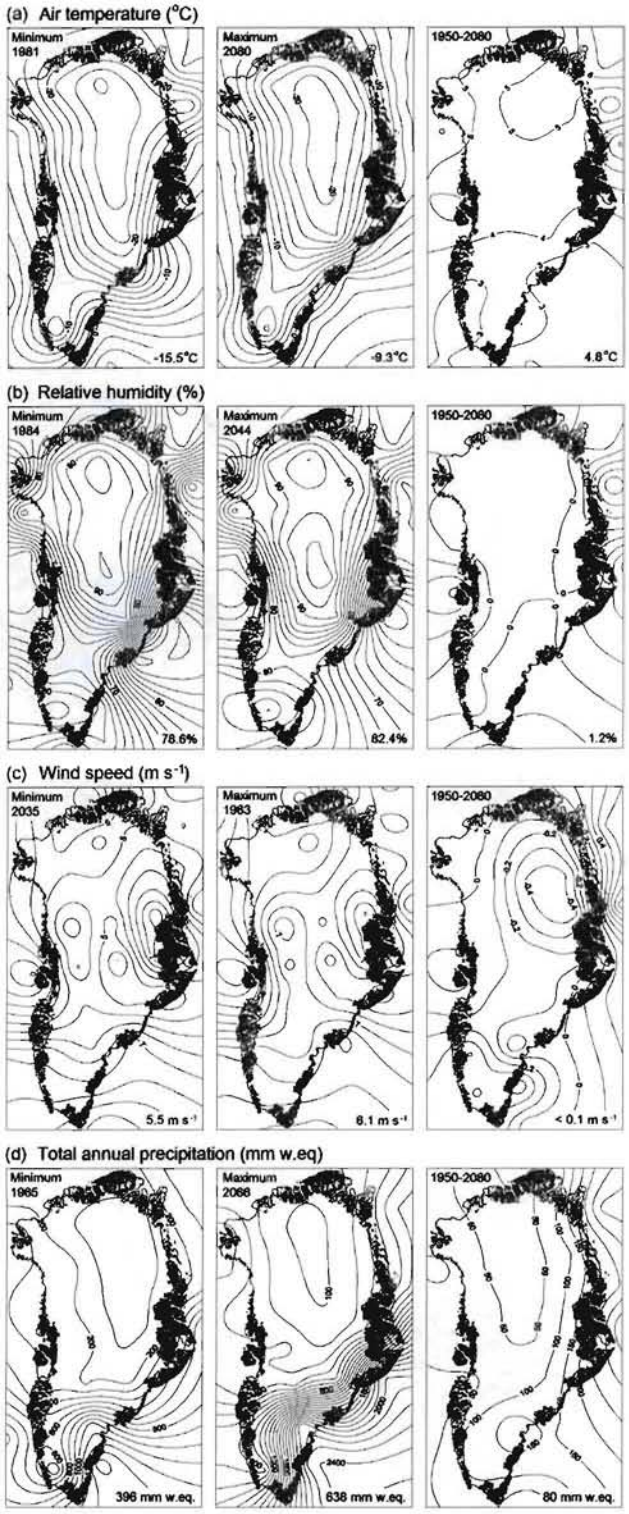

Figure 5: *Greenland HIRHAM4 RCM calibrated annual minimum average, annual maximum average, and average annual trend difference from 1950 through 2080 for the parameters: (a) air temperature, (b) relative humidity, (c) wind speed, and (d) precipitation. The years for the annual minimum and maximum are mentioned for each parameter.*

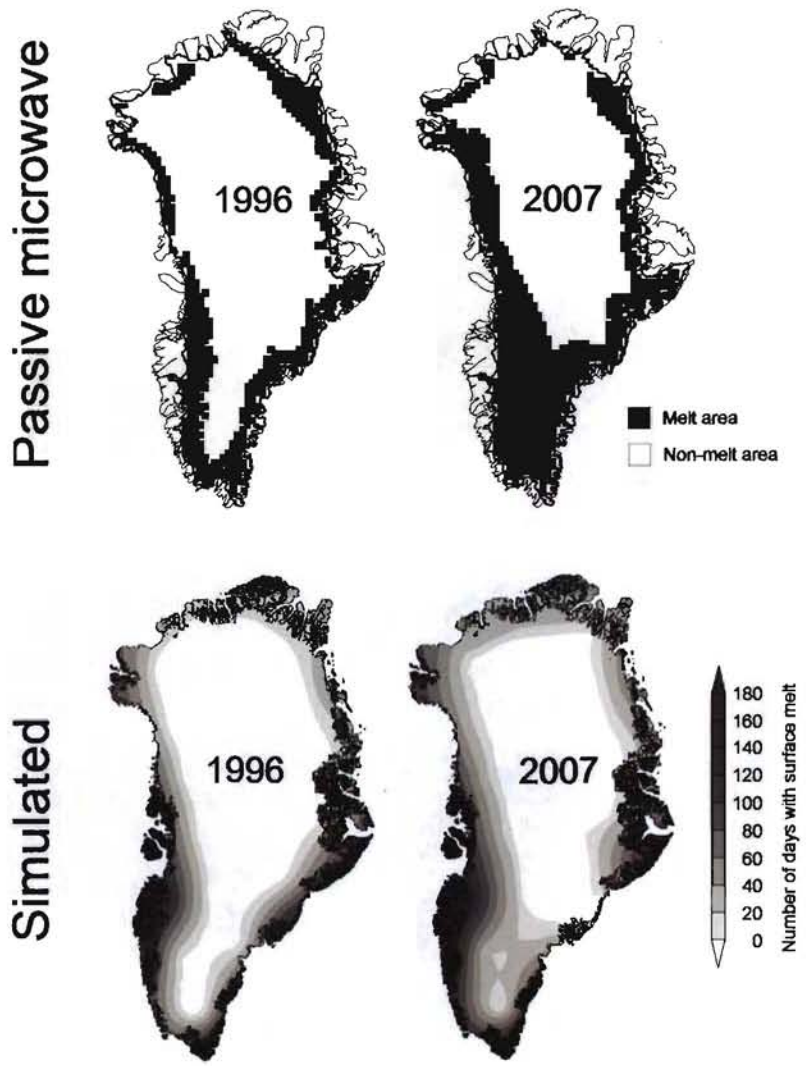

Figure 6a: *The GrIS maximum melt extent based on passive microwave satellite-derived observations and SnowModel simulations for the years 1996 (second lowest melt extent since the satellite observations began in 1979 (only 1992 is smaller than the 1996-melt extent) and 2007 (greatest melt extent since the satellite observations began). The simulated melt extent includes number of days with surface melt.*

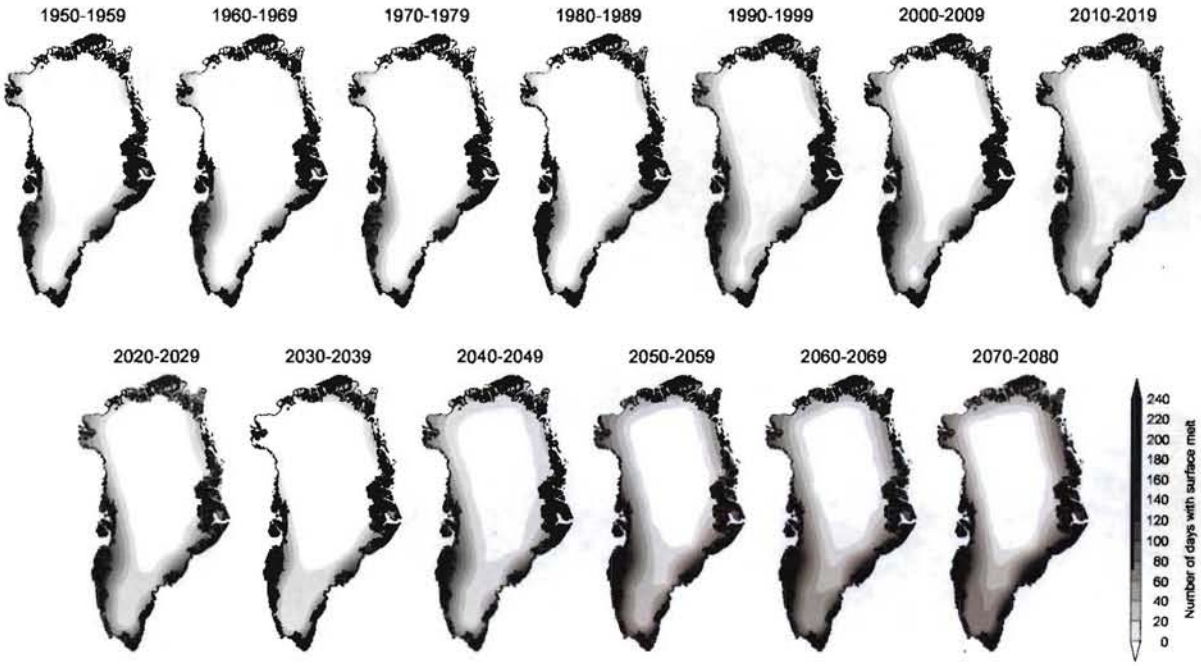

Figure 6b: *Average maximum decadal melt extent from 1950–1959 through 2070–2080, including the number of days with surface melt.*

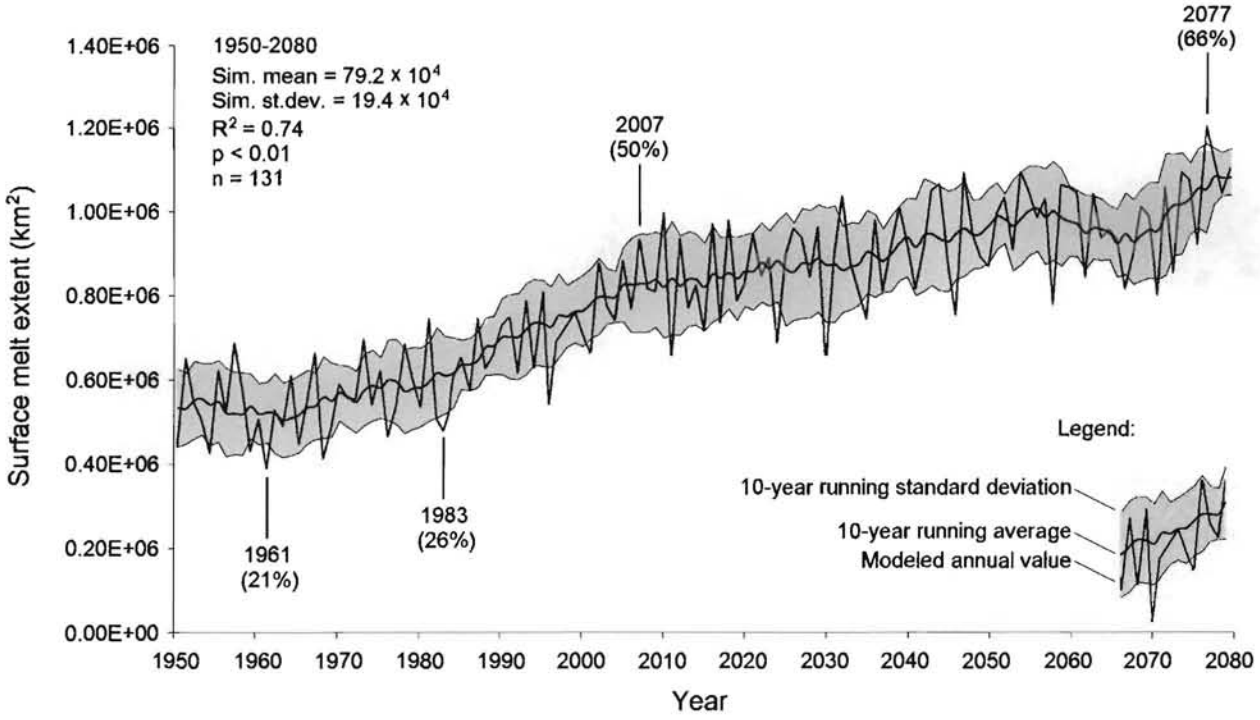

Figure 6c: *Time series for the simulated GrIS surface melt extent from 1950 through 2080. The percentage of total modeled melt extent is shown for the four years: 1961 (the year with the lowest melt extent in the simulation period: 1950–2080), 1983 (lowest melt extent since the satellite observations began in 1979), 2007 (greatest melt extent since the satellite observations began), and 2077 (the year with the highest melt extent in the simulation period).*

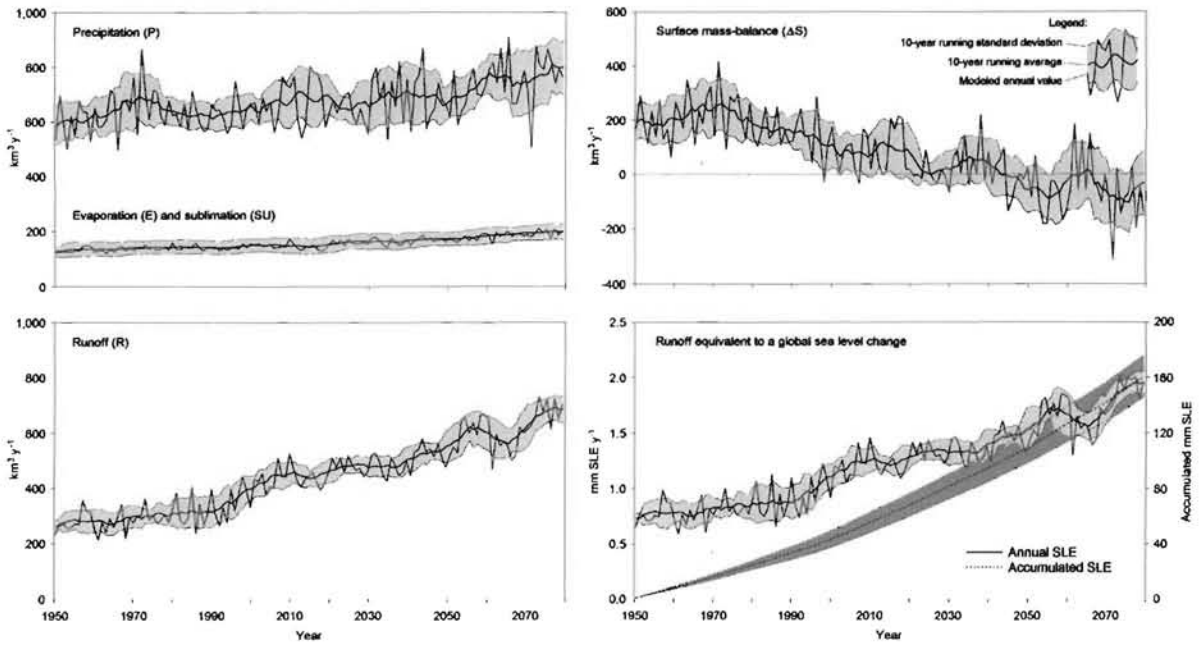

Figure 7: *Time series for the simulated GrIS precipitation (P), evaporation and sublimation (E+SU), surface mass-balance (ΔS), runoff (R), and annual and accumulated contribution to the global sea level change for the period 1950–2080.*

Table 1: *Meteorological input data for the Greenland SnowModel simulations. Meteorological station data on the Greenland Ice Sheet (GrIS) (Station numbers 1–15, and 26) were provided by CIRES, University of Colorado at Boulder, coastal meteorological station data (Station numbers 16–18, and 20–25) by the Danish Meteorological Institute (DMI), and the Zackenberg meteorological station (Station number 19) by Danish National Environmental Research Institute and University of Copenhagen.*

Meteorological Station Number	Meteorological Station Name	Location: (degrees and minutes)	Data time period (year, month, and day)	Altitude (m a.s.l.)	Station used for calibration (C) or validation (V)
1	NASA-U	73°50′31″N; 49°29′54″W	1998-1-1 to 2005-5-29	2,369	C
2	GITS	77°08′16″N; 61°02′24″W	1999-5-7 to 2005-5-14	1,869	C
3	Humboldt	78°31′36″N; 56°49′50″W	1998-1-2 to 2005-6-23	1,995	V
4	Summit	72°34′47″N; 38°30′18″W	1999-9-1 to 2005-8-31	3,208	V
5	Tunu-N	78°00′59″N; 33°59′00″W	1996-5-17 to 2003-11-7	2,052	C
6	DYE-2	66°28′48″N; 46°16′44″W	1996-5-25 to 2003-11-15	2,165	C
7	JAR1	69°29′51″N; 49°41′16″W	1996-6-20 to 2005-12-10	962	V
8	Saddle	65°59′58″N; 44°30′03″W	1997-4-20 to 2004-10-10	2,456	V
9	South Dome	63°08′56″N; 44°49′02″W	1996-4-23 to 2004-10-12	2,901	C
10	NASA-E	75°00′02″N; 29°59′50″W	1997-5-3 to 2004-10-23	2,614	C
11	NGRIP	75°05′59″N; 42°19′57″W	1997-7-9 to 2004-12-29	2,950	C
12	NASA-SE	66°28′45″N; 42°29′56″W	1998-4-24 to 2005-5-25	2,393	C
13	KAR	69°41′58″N; 33°00′21″W	1998-5-18 to 2005-6-7	2,579	C
14	JAR2	69°25′09″N; 50°03′55″W	1999-6-2 to 2005-8-31	542	C
15	JAR3	69°23′40″N; 50°18′36″W	2001-1-1 to 2004-5-24	283	C
16	Hall Land	81°41′00″N; 59°57′00″W	1995-9-1 to 1996-8-31	105	C
17	Station Nord	81°36′00″N; 16°39′00″W	1995-9-1 to 2005-8-31	36	V
18	Danmarkshavn	76°46′00″N; 18°40′00″W	1995-9-1 to 2005-8-31	11	V
19	Zackenberg	74°28′10″N; 20°34′20″W	1997-9-1 to 2005-8-31	43	C
20	Ittoqqortoormiit	70°29′00″N; 21°57′00″W	1995-9-1 to 2005-8-31	66	V
21	Tasiilaq	65°36′00″N; 37°38′00″W	1995-9-1 to 2005-8-31	44	C
22	Ikerasassuaq	60°03′00″N; 43°10′00″W	1995-9-1 to 2005-8-31	88	V
23	Nuuk	64°10′00″N; 51°45′00″W	1995-9-1 to 2005-8-31	80	C
24	Aasiaat	68°42′00″N; 52°45′00″W	1995-9-1 to 2005-8-31	88	C
25	Kitsissorsuit	74°02′00″N; 57°49′00″W	1995-9-1 to 2005-8-31	40	C

Table 2: *User-defined constants used in the SnowModel simulations (see Liston and Sturm (1998) for parameter definitions).*

Symbol	Value	Parameter
C_v		Vegetation snow-holding depth (equal surface roughness length) (m)
	0.50	- Barren
	0.15	- Grassland
	1.00	- Mixed forest
	0.50	- Mixed tundra
	0.30	- Shrubland
	0.01	- Snow
	0.01	- Ice
	0.50	- Wooded tundra
	0.50	- Wooded wetland
	0.01	- Water (ocean and lake)
f	500.0	Snow equilibrium fetch distance (m)
U_{*_t}	0.25	Threshold wind-shear velocity (m s^{-1})
dt	1	Time step (day)
$dx = dy$		Grid cell increment used at different simulations (km)
	0.1	- Model validation at Mittivakkat and Zackenberg catchments
	5.0	- Entire Greenland simulation
α		Surface albedo
	0.8	- Snow
	0.4	- Ice
ρ		Surface density (kg m^{-3})
	280	- Snow
	910	- Ice

Table 3: *Simulated rank-ordered GrIS mean summer air temperature (June-July-August) and summer anomaly for 1950 through 2080.*

Rank	Year	Absolute summer air temperature, °C	Summer anomaly, °C
1	2074	0.58	2.71
2	2078	0.46	2.59
3	2076	0.42	2.55
4	2080	0.17	2.29
5	2066	0.08	2.21
6	2063	-0.13	2.00
7	2075	-0.21	1.91
8	2060	-0.37	1.76
9	2073	-0.39	1.74
10	2069	-0.41	1.71
122	1992	-3.43	-1.31
123	1952	-3.46	-1.34
124	2018	-3.50	-1.38
125	1954	-3.58	-1.46
126	1965	-3.59	-1.47
127	1960	-3.60	-1.47
128	1951	-3.61	-1.48
129	1953	-3.63	-1.51
130	1950	-3.66	-1.53
131	1963	-3.88	-1.75
1950–2080 average and standard deviation		-2.12±1.06	0.00
Minimum		0.58	-1.75
Maximum		-3.88	2.71
Range		4.46	4.46
Average change (°C)		3.14	

Table 4: *Decadal GrIS MAAT, surface melt extent, melt index (above 2,000 m a.s.l.), precipitation (P), evaporation and sublimation (E+SU), runoff (R),surface mass-balance (ΔS), ELA, runoff (R), specific runoff (Rs), runoff equivalent to a global sea level rise from 1950 through 2080. The runoff values do not include hydro-glacio processes such as sudden release of bulk water.*

	1950-1959	1960-1969	1970-1979	1980-1989	1990-1999	2000-2009	2010-2019	2020-2029	2030-2039	2040-2049	2050-2059	2060-2069	2070-2080*	Average and standard deviation
MAAT, °C	-14.8 ±0.4	-14.3 ±0.5	-13.9 ±0.4	-14.1 ±0.7	-13.8 ±0.5	-13.5 ±0.7	-13.5 ±0.6	-13.0 ±0.5	-12.4 ±0.5	-11.9 ±0.3	-11.5 ±0.6	-10.5 ±0.6	-10.1 ±0.5	-12.9 ±1.5
Passive microwave satellite-derived surface melt extent, 10^6 km^2	-----	-----	-----	0.484	0.678	0.774†	-----	-----	-----	-----	-----	-----	-----	0.645††
Surface melt extent, 10^6 km^2 and %	0.469 (26)	0.510 (28)	0.586 (32)	0.617 (34)	0.737 (40)	0.797 (43)	0.838 (46)	0.882 (48)	0.874 (48)	0.934 (51)	0.995 (54)	0.956 (52)	1.025 (56)	0.792 ±0.194
Melt index above 2,000 m a.s.l., km^2 × days 10^6	1.42± 1.34	1.48± 1.27	1.51± 1.20	1.72± 1.29	1.52± 1.14	1.63± 1.28	1.76± 1.45	2.25± 1.27	2.51± 1.42	2.71± 1.31	2.58± 1.30	2.64± 1.43	3.38± 1.41	2.09± 1.62
ELA, m a.s.l.	1,158 ±343	1,151 ±274	1,257 ±201	1,312 ±295	1,238 ±356	1,367 ±281	1,328 ±454	1,575 ±268	1,608 ±428	1,754 ±309	1,790 ±314	1,919 ±430	2,056 ±413	1,520 ±776
Precipitation (*P*), km^3 y^{-1}	600.1 ±68.7	635.9 ±67.8	683.1 ±92.5	618.7 ±47.9	637.1 ±55.6	663.7 ±62.0	692.8 ±99.3	650.0 ±39.9	690.9 ±102.0	698.3 ±96.1	691.8 ±69.5	762.4 ±83.0	770.2 ±100.6	677.3 ±89.7
Evaporation and Sublimation (*E+SU*), km^3 y^{-1}	137.6 ±17.5	109.4 ±16.0	142.3 ±14.4	143.2 ±16.5	148.2 ±15.1	135.4 ±14.0	149.1 ±20.0	165.5 ±15.2	170.8 ±19.4	177.6 ±16.8	179.9 ±16.9	189.3 ±19.4	201.8 ±18.9	157.7 ±25.7
Runoff (*R*), km^3 y^{-1}	284.7 ±36.1	270.6 ±39.5	299.5 ±25.9	314.5 ±53.5	353.8 ±59.7	425.4 ±48.1	443.4 ±39.0	482.1 ±26.5	480.9 ±35.9	529.2 ±37.0	589.7 ±66.1	573.0 ±63.3	667.7 ±47.6	442.1 ±134.4
Ablation (*E+SU+R*), Km^3 y^{-1}	422.3 ±45.7	380.0 ±46.1	441.8 ±31.6	457.7 ±53.3	502.0 ±64.8	560.8 ±45.5	592.5 ±52.6	647.6 ±33.8	651.7 ±48.7	706.8 ±45.2	769.6 ±72.9	762.3 ±72.1	869.5 ±60.6	597.3 ±152.7
Surface mass-balance (*ΔS*), Km^3 y^{-1}	177.8 ±71.7	255.9 ±73.2	241.3 ±96.3	161.0 ±53.7	135.1 ±89.4	102.9 ±71.6	100.3 ±92.1	2.4 ±32.8	39.2 ±89.1	-8.5 ±75.8	-77.8 ±84.0	0.1 ±111.1	-99.3 ±103.1	79.3 ±128.9
Specific runoff (*Rs*), l s^{-1} km^{-2} y^{-1}	4.9 ±0.6	5.2 ±0.7	5.2 ±0.4	5.4 ±0.9	6.1 ±1.0	7.4 ±0.8	7.7 ±0.7	8.3 ±0.5	8.3 ±0.6	9.1 ±0.6	10.2 ±1.1	9.9 ±1.1	11.5 ±0.8	7.6 ±2.3
Runoff equivalent to the global sea level change, mm SLE y^{-1}	0.79 ±0.10	0.75 ±0.11	0.83 ±0.05	0.87 ±0.18	0.98 ±0.16	1.18 ±0.16	1.23 ±0.06	1.34 ±0.07	1.33 ±0.09	1.47 ±0.10	1.63 ±0.08	1.59 ±0.12	1.85 0.08±	1.22 ±0.37
Accumulated runoff equivalent to the global sea level change, mm SLE y^{-1}	7.9	15.4	23.7	32.4	42.2	54.0	66.3	79.6	92.9	107.6	123.9	139.8	160.4	160.4

* The average values are based on 11 years of data, other wise only 10 years are used for each decade from 1950–1959 through 2060–2069, † average passive microwave satellite-derived surface melt extent for the period 2000 through 2007, and †† average passive microwave satellite-derived surface melt extent for the period 1980 through 2007.

Table 5: *Different GrIS surface water balance studies, including parameters for precipitation (P), runoff (R), and surface mass-balance (ΔS) for the period 1995 through 2004, compared with the present HIRHAM4 RCM-SnowModel study.*

	Box et al. 2006	Fettweis 2007	Hanna et al. 2008	Mernild et al. 2008a	RCM-SnowModel
Precipitation (P), $km^3\ y^{-1}$	654.0±36.4	641.2±59.9	655.4±53.5	635.9±35.2	650.2±53.5
Runoff (R), $km^3\ y^{-1}$	395.7±61.1	367.2±92.2	339.3±63.0	387.4±63.3	398.5±45.5
Surface mass-balance (ΔS), $km^3\ y^{-1}$	160.3±69.4	263.3±138.5	316.1±116	141.0±84.7	109.3±88.9